

Bulletin of the Seismological Society of America

Vol. 66

February 1976

No. 1

DYNAMIC MOTIONS NEAR AN EARTHQUAKE FAULT: A THREE-DIMENSIONAL SOLUTION

BY PAUL G. RICHARDS

ABSTRACT

The rupture process occurring during an earthquake is described here in terms of one of the few known solutions to a problem of brittle fracture, in which rupture originates at a point, and spreads over a fault plane, initiating shearing motions. Using a stress-relaxation model with a particular geometry of rupture growth, stresses and displacements can readily be found throughout the medium in which rupture is taking place. The qualitative and quantitative properties of this fracture solution can give considerable assistance in interpreting records of strong ground motion, and provides insight into the processes taking place at an earthquake source.

It is shown that rupture speeds are likely to lie between the Rayleigh-wave and shear-wave speeds, that temperatures can be raised substantially by faulting, and that the ratio of particle velocity to stress drop is approximately proportional to rupture velocity. In order to obtain the rupture velocity in rock mechanics experiments, measurement of displacement normal to the fracture surface is recommended.

INTRODUCTION

Earthquakes are the immediate result of some stress-relaxation process, which spreads rapidly in time over a zone in which stress has previously been slowly accumulating. Evidence that this is so has been growing since the well-known work of Reid (1910) on the 1906 San Francisco earthquake, and his results, amply supported by research since his time, indicate that the relaxation process commonly involves rupture and shear failure across a planar fault surface. This paper describes an earthquake source model which fits the observed kinematics of such ruptures, which is also dynamically satisfactory in terms of the stresses prevailing at and near the earthquake focus, and which permits the solution and computation of all source motions and radiated motions due to the rupture process.

Present theories of the earthquake source are still inadequate to explain many features observed on seismograms. For example, we might suppose that an earthquake is due to motion being initiated at a point on some fault surface within the Earth, that the rupture spreads over the fault surface, and that the rupture stops at some later time. This type of earthquake model can result in seismograms with extremely simple, short, body-wave pulses, having prominent features associated with details of just how motion stops on the fault surface itself (Savage, 1966). Such stopping phases have been identified for some events (Savage, 1965), and short body-wave pulses are occasionally observed (Davies and

Ziolkowski, 1971; Douglas *et al.*, 1974). Yet it must be said that stopping phases are not usually evident on seismograms, and pulse shapes from earthquakes are often complex (even for favorable propagation paths), presumably because the time history of motions at the earthquake source can be very different, from event to event.

Whether an earthquake generates short body-wave pulses, or whether the earthquake is a rapid sequence of small fracture events (leading to complex records), there is a general need for understanding how dynamic shearing motions develop and grow on a fault surface, once they have been initiated by rupture. Many published attacks on this problem are still far from providing a useful solution, because all of the idealizations (i.e., earthquake models) used appear to be too restrictive. Thus, many authors have examined two-dimensional models, in which the rupture front nucleates and moves as a line (Kostrov, 1966; Burridge, 1969; Hanson *et al.*, 1974; Ida and Aki, 1972; and Achenbach and Abo-Zena, 1973). We find below that many characteristics of the earthquake source demand a three-dimensional analysis. Another common approach, initiated by Aki (1968) and Haskell (1969), involves the specification of relative displacements across a rupturing fault, and uses a Green's function integral to calculate the resulting motions set up away from the source. This method is based on work of Burridge and Knopoff (1964), who showed that specification merely of the relative motions across a fault surface permits an explicit solution to be stated for displacement throughout an elastic medium. Unfortunately, their powerful result is not useful without first knowing the temporal and spatial dependence of relative shearing motions taking place across the fault. This motion is itself part of the solution one is trying to find. Ida and Aki (1972) have given many examples (for certain two-dimensional problems) of how the shear *stress* on a fault surface behaves for different assumptions about shearing *motions* across the fault. However, for the plane strain problems of most interest, we still do not know what shearing motions are appropriate for most standard fracture criteria (which are usually given as constraints on stress). The most commonly assumed shearing motion, the 'dislocation ramp' of Haskell (1969), does not appear to have been examined in terms of the time history of shearing stresses. However, the work of Ida and Aki (1972) for antiplane strain problems, and the solution discussed below, indicate that the Haskell ramp dislocation is completely inappropriate in terms of the physics of material rupture, and has unacceptable time histories of shear traction.

This paper reviews and develops properties of a stress-relaxation model of an earthquake, in which rupture begins at a point and spreads steadily over a fault surface. The dynamic constraints on motion are given in terms of shear stress on the fault, using concepts of dynamic friction. Elements of the model have previously been described as an exercise in fracture mechanics by Kostrov (1964), Burridge and Willis (1969), and Richards (1973). The first two of these papers gave formal solutions for motion within the faulted medium, and the third showed how numerical results could rapidly be computed in practice. The present paper has five objectives: to point out several surprisingly simple physical features of the earthquake model; to demonstrate that significant rises in temperature are likely on a rupturing fault surface; to find likely values for the rupture velocity; to give a quantitative picture of the motions at and near the active focus of an earthquake; and to evaluate the relationship between stress drop and particle velocity on a fault surface, for different speeds of rupture propagation.

DESCRIPTION OF EARTHQUAKE MODEL

We consider a homogeneous elastic medium, and take an earthquake source to involve a plane (fault) surface, across which discontinuous displacements arise in direc-

tions parallel to the fault. Such a discontinuity is often referred to as a “dislocation.” However, this can lead to confusion with the meaning associated with a dislocation in crystallography, so the term “slip” is preferable, although we must extend the common usage by taking slip to be a varying function of time and of position on the fault surface. Since rupture involves shear failure, the slip must satisfy not only a kinematic description of shearing motion across a fault, but also dynamic constraints on the components of traction across the fault surface. The physics of the faulting process determine these constraints, and we shall assume that shear stresses on the new fault surface, after a rupture front has passed by and initiated relative motion between opposite faces of the fault, are entirely frictional, being proportional to the normal stress. This physical assumption is much simpler to work with than might be expected, since it may be shown [by symmetries in the displacement formulas of Haskell (1969) for the radiation from a finite fault] that the normal stress stays constant throughout the rupture process. That is, the normal stress cannot be changed on a fault surface (within an infinite homogeneous medium) by *any* choice of the slip function. The shear stress on the new fault surface is, therefore, time-independent.

The above remarks are relevant to problems even with an inhomogeneous initial stress, and unsteady rupture propagation. The particular source to be taken up below is further simplified by dropping these two features, thereby yielding a tractable problem, although one which still is of practical relevance to our understanding of the rupture process in earthquakes.

Specifically, assume initially a state of uniform stress σ^0 , and suppose that a plane shear crack nucleates at the origin, at time $t = 0$. The fault surface $S(t)$ is defined in cartesian coordinates by the ellipse

$$S(t) = \{z = 0: x^2/\sigma^2 + y^2/v^2 \leq t^2\}$$

which (see Figure 1) has axes growing steadily at speeds σ and v , each less than, or equal to, the shear-wave speed β . The shear stresses across plane $z = 0$ are influenced by waves emanating from the point of nucleation, but after arrival of the rupture they drop to new values, constrained to be constant over $S(t)$. Note that, because of radiation from previous growth of the crack, we do not immediately know the value (at a given point in the fault plane) the stress drops down *from*, at the arrival of rupture. We know a constraint only on what the stress drops *to*, namely, that the shear stress drops to a value which is constant over S .

To describe the problem further, let \mathbf{u} be displacement away from the initial (pre-stressed, static) position, with τ as the stress tensor due to \mathbf{u} (so that $\sigma^0 + \tau$ is the total stress). To set up a boundary value problem, note that constancy of normal stress across the fault plane implies

$$\tau_{zz} = 0 \quad \text{everywhere on } z = 0. \quad (1)$$

The assumption that shear stresses on the new fault surface are purely frictional implies

$$(\tau_{zx}, \tau_{yz}) = (\sigma_{zz}^0 \mu_d \cos \psi - \sigma_{zx}^0, \sigma_{zz}^0 \mu_d \sin \psi - \sigma_{yz}^0) \quad \text{on } S(t), \quad (2)$$

in which ψ specifies the frictional force direction (opposite to the direction of slip), and μ_d is the coefficient of dynamic friction. It follows that shear stresses are constant over $S(t)$ if and only if at least one of the following is true: the initial normal stress σ_{zz}^0 is zero, the friction coefficient μ_d is zero (e.g., if the fault surfaces are molten), or slip takes place in the same fixed direction everywhere on the fault, so that ψ is constant.

It may be expected that our problem of solving for the vector displacement everywhere in the medium will require three conditions over the total boundary surface $z = 0$. Equation (1) is one such condition, and (2) is two conditions for a part of the boundary. Two more conditions for the remaining part of the boundary can also be stated. They are conditions on the shearing displacements, which Haskell's (1969) formulas show to be odd functions of z , the distance from the fault. Since they are also continuous except across $S(t)$, we conclude

$$u_x = u_y = 0, \quad \text{on } z = 0 \text{ but off } S(t). \quad (3)$$

Solving for the elastic motion, conditioned by (1), (2) and (3), therefore, appears to be a mixed boundary value problem. However, a greatly simplified ordinary boundary value problem can instead be set up, using the work of Burridge and Willis (1969), who found the discontinuity in shearing displacements across $S(t)$, for the present problem of an elliptical crack. They did this essentially by guessing the temporal and spatial dependence of the slip, subsequently verifying that all necessary properties of this brittle fracture problem are correctly reproduced by the guess. Their work implies that

$$(u_x, u_y) = \begin{cases} (0, 0) & \text{on } z = 0^+ \text{ but off } S(t) \\ (a, b)(t^2 - x^2/\sigma^2 - y^2/\nu^2)^{1/2} & \text{on } z = 0^+ \text{ and } S(t). \end{cases} \quad (4)$$

Note that particle displacement at the origin (point of nucleation) has components (at, bt) after rupturing, so the constant (a, b) velocities are just particle velocities for the center of the crack. Conditions (1) and (4) are now in the form which establish a boundary value problem for elastic radiation into $z \geq 0$. Radiation into $z < 0$ can be determined by symmetry, or by setting up boundary values on $z = 0^-$.

Burridge and Willis (1969) have shown that shear stress jumps (τ_{zx}, τ_{yz}) are indeed constant in time and space on $S(t)$, being proportional to the source particle velocities, i.e.,

$$\tau_{zx} \propto a, \quad \text{and} \quad \tau_{yz} \propto b, \quad \text{on } S(t). \quad (5)$$

From equation (4), the direction of slip is fixed in time and space over $S(t)$, so the direction of frictional force (given by angle ψ) is fixed, and it is indeed appropriate to consider this earthquake source as one which [via equation (2)] is constrained by dynamic friction. A brief description is given below of the radiation solution for the case $b = 0$, i.e., for relief of initial stress component σ_{zx}^0 . [It follows from (2), (4) and (5) that $\psi = 0$ and $\sigma_{zy}^0 = 0$, so the case $b = 0$ involves no loss of generality: it arises when the x -axis is taken in the direction of maximum initial shear, which subsequently becomes the direction of slip.]

SOLUTION METHOD FOR MOTIONS THROUGHOUT THE MEDIUM

Although formal displacement solutions may be set up for many interesting problems of fracture, few representations permit calculation of the motion without major and sophisticated computation—the effort involved suppressing most attempts. Thus, knowledge of the slip (4) permits a surface integral to be written down for the radiation (Haskell, 1969). The integrand, however, is singular, and although Anderson and Richards (1975) have been able to achieve numerical stability for displacements, it is unlikely the method could be used for accelerations. Burridge and Willis (1969) have obtained a formal solution for the present problem, also involving a surface integral, but their representation appears computationally even more intractable.

The present method, outlined below and given in detail by Richards (1973), gives acceleration and stress-rates, at all positions and times, in terms of single integrals plus algebraic expressions. The integrands are nonsingular, and the solution is readily programmed.

Major steps in the method, based on Cagniard-de Hoop theory for moving sources, are

(a) Fourier transformation of x and y ; Laplace transformation of t

$$f(x, y, z, t) \rightarrow \overset{\approx}{f}(k, \ell, z, s),$$

where f is any dependent variable (such as a displacement component) of interest. Boundary conditions on $z = 0$ are then

$$\overset{\approx}{\tau}_{zz} = 0, \overset{\approx}{u}_x = \frac{4\pi a \sigma v}{[s^2 + k^2 \sigma^2 + \ell^2 v^2]^2}, \overset{\approx}{u}_y = 0.$$

(b) Transformation of the wave equation, and use of potentials, to derive algebraic expressions for $\overset{\approx}{\mathbf{u}}(k, \ell, z, s)$. The double Fourier inverse transform is taken, yielding the forward Laplace transform as an explicit double integral over the whole (k, ℓ) plane. A rotation and stretch of the (k, ℓ) plane to variables (w, q) is carried out via the de Hoop transformation

$$k = (s/\alpha) [q \cos \phi - w \sin \phi], \ell = (s/\alpha) [q \sin \phi + w \cos \phi],$$

where α is the P -wave speed. The Laplace-transformed P -wave component of displacement at position \mathbf{x} then has the form

$$\bar{u}_p(\mathbf{x}, s) = (1/s^2) \int_0^\infty dw \int_{-\infty}^\infty dq \mathbf{F}(q, w, \phi) \exp(-st), \quad (6)$$

where \mathbf{F} is known,

$$t = t(q, w, \theta) \equiv [-iq \sin \theta + (1 + q^2 + w^2)^{1/2} \cos \theta](R/\alpha),$$

and the spherical polars (R, θ, ϕ) for \mathbf{x} are shown in Figure 1. It can be shown that only the positive real q axis is needed for the integration in (6). There is a similar expression for the S -wave component.

(c) Application of Cagniard's method, turning the q integral into the Laplace transform of the w integral, so that displacement in the time domain is recognized as a single integral over w . A complication arises, due to singularities of the integrand \mathbf{F} , as shown in Figure 2. This is a diagram of the complex q plane; it shows that between the real-axis path of integration needed in (6), and the Cagniard path (on which the exponent $t(q, w, \theta)$ in (6) is real), the integrand has a pole. In fact, it is a second-order pole, denoted, say, by $q_{\sigma v}$, and is due to the moving nature of the source: it is necessary to pick up the residues in converting to the Cagniard path, giving the form

$$\begin{aligned} \bar{u}_p(\mathbf{x}, s) = & (1/s^2) \int_0^\infty dw \int_C dt \mathbf{F}(q(t), w, \phi) \exp(-st) dq/dt \\ & + \int_0^\infty dw \mathbf{R}(q_{\sigma v}, w, \phi, s) \exp[-st(q_{\sigma v}, w, \theta)]. \end{aligned} \quad (7)$$

From the first right-hand-side term here, one can invert to the time domain in the usual fashion (i.e., by reversing the order of integration, and recognizing the result as a forward Laplace transform), obtaining a single integral over w . It is remarkable that the second right-hand-side term in (7), which one might have expected to cause difficulty, is already in the form suitable for recognition as the Laplace transform of an identifiable function of time. That is, the inversion (to the time domain) of this second term results merely in an algebraic closed-form expression. This method, an algebraic expression resulting from an integral of residues, was first developed by Gakenheimer and Miklowitz (1969) for solving Lamb's problem with a moving source.

Experience indicates that the acceleration can be sampled at several hundred points within 10 sec of machine time by an IBM 360/95 computer. Although detailed quantitative work is necessary, to evaluate the model as an accurate representation of earthquake faulting, considerable insight into the nature of the solution is gained by first obtaining overall qualitative properties of stresses and displacements within the model.

PROPERTIES OF THE SOLUTION: WAVE FRONTS AND SINGULARITIES

Since the rupture velocities σ and ν do not exceed the shear-wave speed, the only wave fronts generated are simply those spherical wave fronts (spreading with P - and S -wave speeds α and β) which emanate from the origin of rupture itself, and which carry discontinuities in the dilatational and shear-wave fields. These discontinuities are found

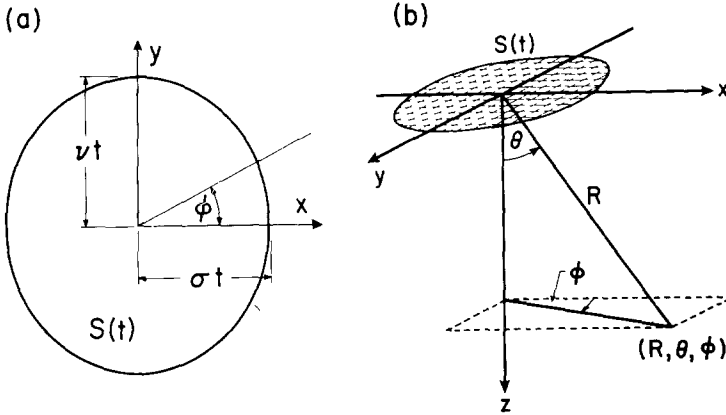


FIG. 1. Parameters for a growing elliptical crack: (a) the plane $z = 0$, seen from the side with $z > 0$; (b) the definition of spherical polar coordinates (R, θ, ϕ) . Azimuth angle ϕ is taken between the plane $y = 0$, and the plane containing the field point and the z -axis.

(Burridge and Willis, 1969; Richards, 1973) to be a step jump in acceleration, with the radiation pattern of a double couple, but modified by directional factors

$$[\alpha^2 - (\sigma^2 \cos^2 \phi + \nu^2 \sin^2 \phi) \sin^2 \theta]^{-2} \quad \text{for } P \text{ waves,}$$

and

$$[\beta^2 - (\sigma^2 \cos^2 \phi + \nu^2 \sin^2 \phi) \sin^2 \theta]^{-2} \quad \text{for } S \text{ waves.}$$

Note that the S -wave factor can become large near the fault plane ($\sin \theta \sim 1$) if σ and/or ν approaches β . Also, the associated high-frequency behavior of displacement amplitude spectra will be like $(\text{frequency})^{-3}$.

The fault motions under discussion have been set up to conform to a simple description of *stress* (on the fault plane), so there is no guarantee that associated *displacements* will also be simple to describe. For example, it might be expected that the fault plane will become warped as rupture proceeds, and that the directions of slip and shear stress will vary over the fault plane. Fortunately, all these complications are absent, and simple properties of both the stress and the displacement fields can be summarized as follows.

(a) That part of the fault surface which is in motion [i.e., $S(t)$] is still a plane, twisted out of the original fault plane $z = 0$ by, e.g., a small angle ϵ which does not change with time. In fact, on $S(t)$, $u_z = \epsilon x$; ϵ is proportional to the stress drop, and has the same sign.

(b) As implied by equations (4) and (5) above, for a drop in the zx stress component alone, slip motion on $S(t)$ is purely in the x direction and $\tau_{yz} = 0$ on $S(t)$. However, for points in the fault plane which have yet to rupture, τ_{yz} need not be zero. This complication is imposed by the three-dimensional nature of the model, and is absent from plane strain solutions.

(c) Waves radiated from a moving fault will set up, throughout the medium, displacements and stresses which in general depend on each of the four coordinates (R, θ, ϕ, t) . However, our model lacks any intrinsic length scale, or time scale, so the temporal and spatial variation of stresses (which initially are constant) cannot be a function of R and t independently. Since the effect of increased distance is merely to expand the time scale, it follows that stresses are dependent on R and t only via the combination t/R , and the stress field may be completely described in terms of the three dimensionless variables $(\theta, \phi, \alpha t/R)$. Stress rates, stress gradients and accelerations are therefore functions of

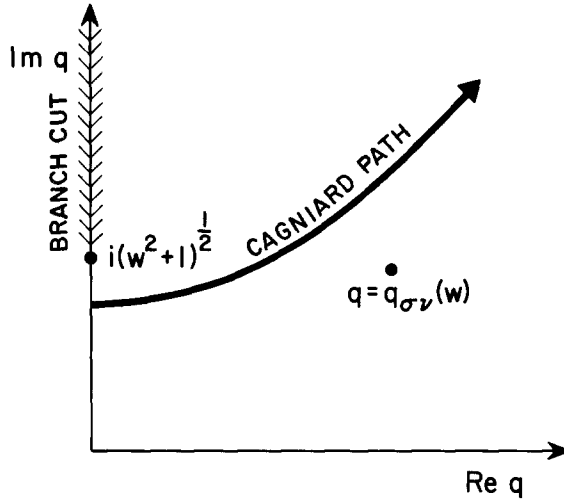


FIG. 2. Branch cut, Cagniard path, and the propagation pole in the first quadrant of the complex q -plane.

$(\theta, \phi, \alpha t/R)$ divided by R , whereas displacements at given $(\theta, \phi, \alpha t/R)$ are proportional to R . Our solution is “self-similar”, in that the propagated pulse retains the same form, at all positions along a given straight line passing through the point of initial rupture on the fault, although its time scale will expand in proportion to distance R .

(d) At any instant of time, the distribution of slip over the fault plane is the same as that which also provides a static solution for the insertion of an elliptical shearing surface into a pre-stressed medium. This is shown below by comparison with Eshelby’s (1957) work. However, for a given dynamic distribution of slip, as equation (4) at a fixed moment of time, this study has shown that a static crack with the same major and minor axes (and the same slip distribution) would have a smaller stress drop.

(e) It is common practice, in describing the fault slip which takes place during an earthquake, to speak of the time function of fault motions. For example, Haskell’s (1969) time function is a ramp, with a certain rise time. The very concept of such a time function implies that the slip can be factorized into a function of position on the fault surface, multiplied by the time function. Such terminology is not applicable to the present slip function (equation 4), for which the spatial and temporal dependences cannot be separated. The time-dependence of this slip is shown for several positions in Figure 3, indicating its hyperbolic nature, with the ramp $u_x = at$ (the motion of the point of nucleation) as the asymptote for all positions.

(f) Around the propagating rupture front of our fault model, there are singularities in stress and particle velocity. The consequences of these concentrations of stress, and their influence on the velocity of rupture, are assessed in the following section. Here, we merely state the asymptotic form of the solution, as $\varepsilon \rightarrow 0$, where

$$\varepsilon = 1 - t(x^2/\sigma^2 + y^2/v^2)^{-1/2} \quad (8)$$

is a dimensionless measure of distance away from the rupture front. (In the plane $z = 0$, ε is positive ahead of the rupture, is zero at the rupture itself, and is negative on the moving part of the fault surface.)

For relief of the zx component of stress, it follows from equation (4) that

$$\dot{u}_x(-2\varepsilon)^{1/2} \sim aH(-\varepsilon) \quad \text{as } \varepsilon \rightarrow 0, \quad (9)$$

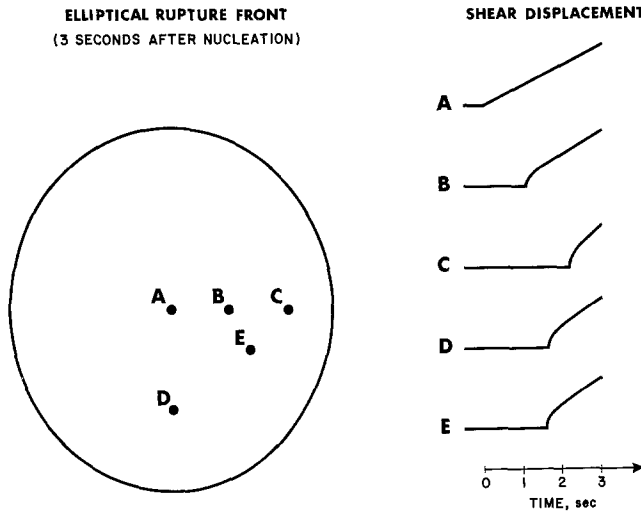


FIG. 3. The time-dependence of slip is shown at five different points on the fault surface, for the first 3 sec after crack nucleation. At point A, the displacement is ramp-like, with slope giving particle velocity at the source. At four other points shown, motion grows hyperbolically, as given by equation (4), with asymptote parallel to the slope at point A.

where a dot ($\dot{}$) denotes the time derivative ($\partial f/\partial t$), and H is the Heaviside step function. Singularities in \dot{u}_y and τ_{zz} are absent on $z = 0$, since these quantities are zero throughout the plane. Quoting from Richards (1973), singularities in the remaining velocity and traction components on $z = 0$ are

$$\dot{u}_z(2\varepsilon)^{1/2} \sim \frac{2\beta^2 Na \cos \phi}{\Sigma \alpha^2 F^{1/2} B_s} \left[\frac{1}{2} \alpha^2 / \beta^2 + B_s^2 - B_p B_s \right] H(\varepsilon) \quad (10)$$

$$\tau_{zx}(2\varepsilon)^{1/2} \sim \frac{4\mu\beta^2 a}{\Sigma^2 \alpha^3 F B_s} \left[(B_p - B_s) B_s N^2 \cos^2 \phi + \frac{1}{4} (\Sigma^2 B_s^2 F - N^2 \cos^2 \phi) (\alpha^2 / \beta^2) \right] H(\varepsilon) \quad (11)$$

$$\tau_{yz}(2\varepsilon)^{1/2} \sim \frac{4\mu\beta^2 a \cos \phi \sin \phi}{\alpha^3 F B_s} \left[B_s B_p - B_s^2 - \frac{1}{4} (\alpha^2 / \beta^2) \right] H(\varepsilon), \quad (12)$$

where μ is the rigidity, and all capital letter symbols are dimensionless quantities given by

$$\Sigma = \sigma/\alpha; \quad N = v/\alpha; \quad F = \Sigma^2 \sin^2 \phi + N^2 \cos^2 \phi;$$

$$B_p^2 + 1 = B_s^2 + \alpha^2 / \beta^2 = (\Sigma^4 \sin^2 \phi + N^4 \cos^2 \phi) / (\Sigma^2 N^2 F).$$

Since the singularities (9) to (12) describe *local* properties of the motion at points near the rupture front, it is instructive to work with a coordinate system related naturally to the local geometry. Figure 4a shows such a system, using directions of the normal, the tangent, and the bi-normal (i.e., the z axis). Tensor components (τ_{zx} , τ_{yz}) are rotated to

$$\begin{aligned}\tau_{zn} &= \tau_{zx} \cos \chi + \tau_{yz} \sin \chi. \\ \tau_{tz} &= -\tau_{zx} \sin \chi + \tau_{yz} \cos \chi.\end{aligned}\quad (13)$$

Letting v_n be the velocity of rupture, in direction \mathbf{n} , one finds

$$v_n = (\sigma v/\alpha)[F/(\Sigma^4 \sin^2 \phi + N^4 \cos^2 \phi)]^{1/2}, \quad (14)$$

which is simply related to B_p and B_s .

We are now in a position to resolve the local motion into components of plane strain (u_n and τ_{zn}) and antiplane strain (u_t and τ_{tz}). Results for the singularities are

$$\begin{aligned}\dot{u}_n(-2\varepsilon)^{1/2} &\sim \frac{v_n N \cos \phi a}{\Sigma F^{1/2} \alpha} H(-\varepsilon) \\ \tau_{zn}(2\varepsilon)^{1/2} &\sim \frac{4\mu\beta^2 N a \mathcal{R}(v_n)}{\alpha^2 v_n F^{1/2} \Sigma B_s} \cos \phi H(\varepsilon)\end{aligned}\quad (15)$$

as $\varepsilon \rightarrow 0$, where

$$\mathcal{R}(v_n) \equiv B_s B_p - B_s^2 - \frac{1}{4}(\alpha^2/\beta^2)(v_n^2/\beta^2)$$

so that \mathcal{R} is the Rayleigh function

$$\begin{aligned}\mathcal{R}(v) &= \frac{\alpha^2}{v^2} \left[\left(1 - \frac{v^2}{\alpha^2}\right)^{1/2} \left(1 - \frac{v^2}{\beta^2}\right)^{1/2} - \left(1 - \frac{v^2}{2\beta^2}\right)^2 \right]; \\ \dot{u}_t(-2\varepsilon) &\sim -\frac{v_n \Sigma \sin \phi a}{N F^{1/2} \alpha} H(-\varepsilon) \\ \tau_{tz}(2\varepsilon)^{1/2} &\sim -\frac{\mu \Sigma v_n a B_s}{N F^{1/2} \alpha^2} \sin \phi H(\varepsilon).\end{aligned}\quad (16)$$

Note that the plane strain-stress singularity (15) will vanish (at positions ϕ around the rupture front) wherever the rupture speed is the Rayleigh-wave speed, and the antiplane strain-stress singularity (16) will vanish wherever the rupture speed is the shear speed (so that B_s is zero). Another important property of equations (15) and (16) concerns the ratio of the strengths of stress and particle velocity singularities. It may be seen that this ratio depends only on local properties of the rupture motion, being $4\mu\beta^2 \mathcal{R}(v_n)/(\alpha v_n^2 B_s)$ for plane strain, and $\mu\beta_s/\alpha$ for antiplane strain, so it is reasonable to conjecture that these ratios are fundamental. They would be expected in any geometry of shearing, not merely in the plane elliptical case with unidirectional slip.

Since this paper assumes a linear relation between stress and strain, it is necessary to justify the use of singularities such as (9) to (12), (15) and (16). They cannot be used to model the actual stresses and particle velocities at the rupture front (or, crack tip) within real materials, since there are stress and strain thresholds above which real materials do not behave in a linear fashion. Clearly the singularities are an analytical artifact,

which we may hope to find convenient in a description of macroscopic properties of the stress concentration. This situation is somewhat analogous to the use of a Dirac delta function to describe the density distribution of a point mass. To see how near the rupture front one may expect linear behavior, we note in (11) and (12) that 4μ is approximately 1 megabar for competent igneous rocks; that particle velocity a is approximately 100 cm/sec in the source region (Brune, 1970); and that $\cos \phi$, B_s , B_p , Σ , N , F are of order unity. With α approximately 5 km/sec, it follows that ϵ must be greater than about 0.01 to keep stresses below 1 kb, i.e., within the linear range. In turn, this implies that

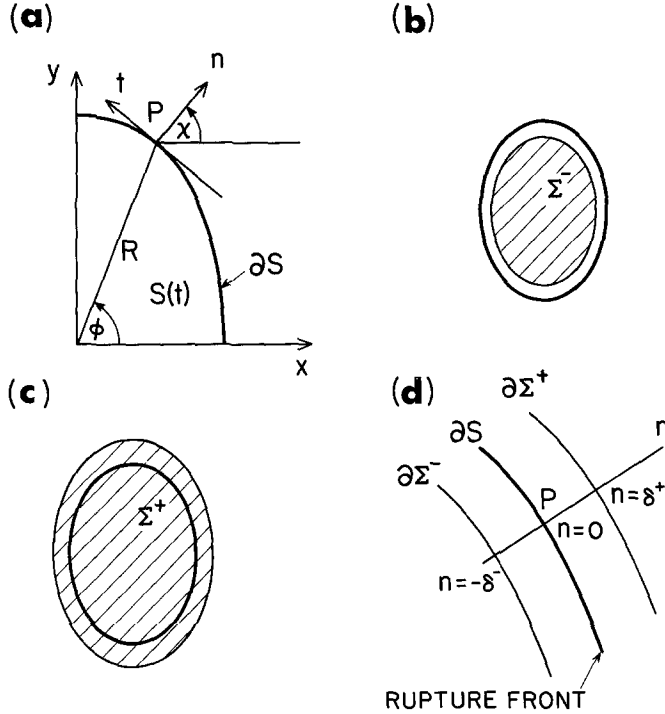


FIG. 4. Four diagrams showing parameters in the fault plane, $\theta = 90^\circ$. (a) Local coordinates n (normal), t (tangential) for a point P at (R, ϕ) in the rupture front, the boundary of $S(t)$. (b) The lined area denotes Σ^- , lying within S . (c) The lined area denotes Σ^+ , covering S . (d) An enlarged view of the vicinity of P , showing part of the strip $\Sigma^+ - \Sigma^-$ covering the rupture front. Symbol ∂ denotes the perimeter (boundary) of a surface.

(9) to (12) can indeed provide valid descriptions of the macroscopic properties of the rupture front, at distances greater than about 1 per cent of the fault radius, away from the rupture front.

The principal physical effect of the dynamic stress singularities lies in their control of the rupture velocity. If the stress just ahead of the rupture front ($\epsilon > 0$) is great enough, then there will be further fracture, and the fault will continue to extend. The rate of extension presumably is controlled by the amount of stress concentration, and the suggestion of early investigators (e.g., Broberg, 1960) was that the rupture velocity is that for which the stress singularity vanishes. In our case of a three-dimensional model of shear, it is possible to make the τ_{yz} singularity (11) vanish for all directions ϕ by taking the circular fault specified by

$$\sigma = v = [8\beta^2(\alpha^2 - 2\beta^2)/(9\alpha^2 - 16\beta^2)]^{1/2},$$

but then the τ_{zx} singularity is still present. Alternatively, if we choose the elliptical model

$$\sigma = \text{Rayleigh-wave speed, and } \nu = \beta,$$

then τ_{xz} is zero in the special directions $\phi = 0$ and $\phi = \pi/2$, but both shear components then have a negative singularity at all intermediate values of ϕ . No choice of σ and ν can be made, for which the τ_{xz} singularity vanishes everywhere.

A resolution of this problem is advanced by examining work done on the fault surface itself — work done against frictional forces and cohesive forces.

WORK DONE ON AN ACTIVE FAULT SURFACE: IMPLICATIONS FOR RUPTURE VELOCITY AND TEMPERATURE RISE

The frictional forces, present on a fault surface undergoing shearing motion, do work which makes the active fault a heat source. McKenzie and Brune (1972) found that melting temperatures were possible for a fault model with infinite rupture speed, and a preliminary study indicates that such temperatures are likely for the plane elliptical shear crack. Work is also done on the fault surface simply to create new surface. This process, better understood for tension cracks than for shearing rupture, has been described by Burridge (1968) in terms of work done against cohesive forces. It is these forces which hold a crystal lattice together, and work must be done against them when a fracture surface is introduced. The amount of work required is unknown: for crystalline quartz, broken in tension, it is a few hundred ergs per square centimeter (Brace and Walsh, 1962), and the surface energy required for reactivating a geological fault in shear is unlikely to be substantially greater than this value. However, even if laboratory measurements were available for the work done in shear against cohesion in various rock-forming minerals, a substantial uncertainty would be involved in extrapolating to values for a geological fault, since the "area" of new fracture should be taken as the total surface area of new fault gouge, and individual gouge particles are presumably formed by tension as well as shear. Where a working value is needed below, the surface energy is taken as 1000 ergs/cm², a relatively high value, but compensated by taking area only as the macroscopically apparent fault surface.

This section describes the way in which the elasticity solution, for motions set up by the plane elliptical shear crack, does work on the underlying fault surface. Two contributions to the work may be distinguished spatially. The first, acting on the fault surface behind the rupture front, is straightforwardly related to frictional heating. The second, due only to singularities in stress and particle velocity, is shown to act precisely at the rupture front itself. Unless special values are adopted for the rupture speeds, the two contributions are of similar magnitude. Physical arguments, based partly on a study of temperature diffusion, are then given to show that rupture speeds all around the rupture front are slightly less than the shear-wave speed.

Frictional work behind the rupture front. The rate at which work is done on a fault surface, by elastic motions taking place during dynamic growth of the fault, is, say, \dot{W} where

$$\dot{W} = \lim_{\Sigma^- \rightarrow S} \iint_{\Sigma^-} (\sigma_{zx}[\dot{u}_x] + \sigma_{yz}[\dot{u}_y]) dS. \quad (17)$$

In this expression, the fault is assumed to lie in the plane $z = 0$; the surface Σ^- (see Figure 4b) is taken within S , to avoid any effect of work done at the rupture front itself; σ_{ij} is the total stress; and square brackets denote a value for the total discontinuity

across the fault. Direct evaluation of (17) is simple for the plane elliptical shear crack, since σ_{zx} is constant, $[\dot{u}_x]$ is known [via doubling the particle velocity deduced from equation (4)], and $[\dot{u}_y] = 0$. The result is

$$\begin{aligned} \dot{W} &= 8\pi\sigma_{zx}\sigma vat^2 \\ &\sim 2.5 \times 10^{23} \times t^2 \text{ ergs/sec.} \end{aligned} \quad (18)$$

if the frictional shear stress σ_{zx} is about 1 kb, the rupture speeds σ and v are about 3 km/sec, the particle velocity a is about 100 cm/sec, and t is in seconds.

It should perhaps be emphasized that σ_{zx} is both the frictional stress and the total shearing stress on the fault acting parallel to the direction of slip. Fault motions with friction have often been modeled by rigid blocks, accelerated parallel to a friction surface against which contact is maintained. In such a model, the analog of total shear stress is total applied force parallel to the friction surface, and this force must exceed the available friction for motion to ensue. However, the mode of faulting considered in this paper is one which accounts for deformation (albeit elastic deformation) right up to the fault surface, avoiding the concept of rigid body motions. The only way for total shearing stress on the moving fault surface to be nonzero, then, is via the mechanism of friction. We shall work with a positive value for the initial stress σ_{zx}^0 , so that equation $\sigma_{zx} = \sigma_{zx}^0 + \tau_{zx}$ indicates the stress jump τ_{zx} is negative everywhere over $S(t)$: τ_{zx} is also constant over $S(t)$, although not elsewhere. That is, shear stress is relieved from value σ_{zx}^0 to the lower (frictional) value σ_{zx} . In this sense, stress drop is the positive quantity $\sigma_{zx}^0 - \sigma_{zx} = -\tau_{zx}$.

The heating effect of faulting will raise temperature T in a homogeneous medium according to the diffusion equation

$$\frac{1}{\kappa} \frac{\partial T}{\partial t} = \nabla^2 T + \frac{A}{K}. \quad (19)$$

Here, κ is the thermal diffusivity ($\sim 7 \times 10^{-3}$ cm²/sec), K is the conductivity ($\sim 2 \times 10^5$ erg/cm² °C sec), and $A = A(\mathbf{x}, t)$ is the rate of heat generation per unit volume. Since the slip is everywhere in the x direction on the fault plane,

$$A = \sigma_{zx}[\dot{u}_x]\delta(z) \quad \text{on } S(t); \quad A = 0 \text{ elsewhere.} \quad (20)$$

It is clear that to solve (19), both the total shear stress and the total jump in particle velocity, $[\dot{u}_x]$, must be known everywhere on $S(t)$. These quantities are known explicitly for our model of an elliptical shear crack. They are also known for the case of a step in stress, applied instantaneously everywhere over a whole plane (Brune, 1970), and the solution of (19) in this case has been described by McKenzie and Brune (1972). These authors found that melting temperatures were possible, and would occur after only a millimeter of slip, if the increment in applied shear stress exceeded about 1 kb. However, the rupture speed in their model is infinite, although they discussed the resulting temperature solution for the case of earthquakes and creep events.

The solution of (19) for the elliptical shear crack is readily obtained when rupture speeds σ and v are equal, e.g., $\sigma = v = v$, so that the rupture is a steadily expanding circle. One finds

$$T = T(R, \theta, \phi, t) = \frac{8(\pi\kappa t)^{1/2}\sigma_{zx}a}{K} F\left(\frac{v}{R \sin \theta}, \frac{\kappa t}{R^2 \sin^2 \theta}, \cos \theta\right) \quad (21)$$

where F is a dimensionless function of three dimensionless variables, and on the fault surface ($\theta = \pi/2$) takes form

$$F(W, D, 0) = \int_0^\infty \left\{ \int_0^1 (1-u) \sin [vW(1-u)] \exp(-Duv^2) u^{-1/2} du \right\} J_0(v) dv.$$

Here, W denotes the wave-like variable vt/R ; D the diffusion-like variable $\kappa t/R^2$, and J_0 the zero-order Bessel function. A more complete discussion is in preparation, but values of F are around 0.9 for $W = 2$, if D is in the range 0.001 to 1. It follows that $T \sim 1100^\circ \times t^{1/2}$ (t in seconds) on the fault surface, halfway between the rupture front ($R = vt$) and the point of nucleation ($R = 0$), if the total shear stress is 100 bars and particle velocity is 10 cm/sec at nucleation. Clearly, temperatures could rise to the melting point, but further work is needed to see if spreading the shearing region over a few centimeters of thickness of fault gouge would change this result significantly (while leaving unchanged the macroscopic fault motions).

Analysis of work at the rupture front. The rupture front may be viewed as the position at which cohesion bonds are broken. The energy needed to achieve this fracture is supplied as a flux, moving from the medium in which the fault propagates, into the region of the moving rupture front itself [see Achenbach, 1974, for detailed analysis]. We shall find that the rate of working against cohesive forces is very small, when compared with the rate available in general from the stress and particle velocities derived in the previous section. The excess available depends on the precise value of rupture velocity, and is presumably dissipated as frictional heating in the vicinity of the rupture front.

We have already obtained an integral (17) for the rate of working on the fault surface behind the rupture front. The rate of working in the vicinity of the moving rupture is, say, \dot{C} where

$$\dot{C} = \lim_{\substack{\Sigma^+ \rightarrow S \\ \Sigma^- \rightarrow S}} \iint_{\Sigma^+ - \Sigma^-} (\sigma_{zx}[\dot{u}_x] + \sigma_{yz}[\dot{u}_y]) d\Sigma. \tag{22}$$

In this integral (see Figure 4b, c, d), Σ^+ is a subregion of the plane of the fault which contains all of $S(t)$ (the part of the fault which is rupturing at time t), including the rupture front; Σ^- is an area contained within $S(t)$. Hence, $\Sigma^+ - \Sigma^-$ is a strip of fault surface which collapses onto the rupture front in the limit. To examine local values of energy balance around the rupture, it is convenient to use the rate of working per unit length of rupture front. If this rate is \dot{D} , then

$$\dot{C} = \oint \dot{D} ds$$

where the integral is taken all around the perimeter of $S(t)$, and

$$\dot{D} = \lim_{\substack{\delta^+ \rightarrow 0 \\ \delta^- \rightarrow 0}} \int_{-\delta^-}^{\delta^+} \sigma_{zx}[\dot{u}_x] dn. \tag{23}$$

The integration variable n here is distance in the fault plane, measured normal to the rupture front (see Figure 4d), and range $-\delta^- \leq n \leq \delta^+$ is taken across the strip $\Sigma^+ - \Sigma^-$. To obtain (23) from (22), we have used the fact that slip is everywhere in the x direction.

For several reasons, it might be expected that the limit in (23) would give a zero value for \dot{D} . Not only is the range of integration vanishingly small, but $[\dot{u}_x]$ is zero in the range $0 < n \leq \delta^+$. In the range $-\delta^- \leq n < 0$, it follows from (9) that $[\dot{u}_x]$ is of order $(-n)^{-1/2}$, and σ_{zx} is constant, so that the integral appears to be of order $\delta^{1/2}$, with zero

limit. However, despite these reasons, \dot{D} is not zero in general, because of the singular nature of the integrand in (23) at value $n = 0$. This integrand has the form

$$\begin{aligned} (\sigma_{zx}^0 + \tau_{zx})[\dot{u}_x] &\propto \left(\text{constant} + \frac{H(\varepsilon)}{\varepsilon^{1/2}} \right) \left(\frac{H(-\varepsilon)}{(-\varepsilon)^{1/2}} \right) \\ &\propto \left(\text{constant} + \frac{H(n)}{n^{1/2}} \right) \left(\frac{H(-n)}{(-n)^{1/2}} \right), \end{aligned}$$

which does yield a significant integral because of the remarkable relation

$$\frac{H(-n)}{(-n)^{1/2}} \frac{H(n)}{n^{1/2}} = \frac{\pi}{2} \delta(n). \quad (24)$$

Here, $\delta(n)$ is the Dirac delta function: the operational property implied in (24) is easily proved from an application of Parseval's theorem, to show that the integral of the left-hand side of (24), over all real n , is $\frac{1}{2}\pi$. The interpretation of (23) is then precisely what we would wish, in terms of the macroscopic consequences of work done against cohesive forces, work which here appears to be done just at the position $n = 0$. For small ε we can relate the dimensioned and dimensionless distances from the rupture front by $n \sim v_n \varepsilon t$, where now t is the time taken for the rupture front to reach a position of interest, say, (R, ϕ) , in the fault plane ($\theta = \pi/2$), so $t = R\alpha F/(\sigma v)$. It then follows from (24), (23), (11), and (9), that

$$\dot{D} = \dot{D}(R, \phi) = \frac{\pi\mu\beta^2 v_n}{\alpha^3 \Sigma^2 N^2 B_s F} \alpha^2 t [\mathcal{A}(v_n) N^4 \cos^2 \phi + \frac{1}{4} B_s^2 (v_n/\beta)^2 \Sigma^4 \sin^2 \phi]. \quad (25)$$

We have obtained this result from the components of stress and particle velocity in cartesian coordinate directions, and the square bracket in (25) is proportional to the τ_{zx} stress singularity (11). It is instructive also to obtain (25) from the work rate $\sigma_{zn}[\dot{u}_n] + \sigma_{tz}[\dot{u}_t]$, since then the term involving $\mathcal{A}(v_n)$ in (25) is seen as the work done on the fault surface by the plane strain component of motion, and the term involving B_s^2 in (25) is the work done by the antiplane strain component.

To appreciate the importance of work done at the rupture front, it is useful to obtain an order of magnitude estimate for \dot{C} . We find that

$$\dot{C} \sim 6\pi^2 |\tau_{zx}| v_n \alpha t^2 \times \{ [(\mathcal{A}v_n) N^4 \cos^2 \phi + \frac{1}{4} B_s^2 (v_n/\beta)^2 \Sigma^4 \sin^2 \phi] / B_s \} \quad (26)$$

in which we have assumed stress drop $|\tau_{zx}| \sim \mu\alpha/\beta$, and $v_n \sim \sigma \sim v \sim \beta \sim \alpha/\sqrt{3}$ in factors other than B_s and \mathcal{A} (which are very sensitive to differences between rupture speed and shear speed). The last factor, within symbols $\{ \}$, is averaged around the perimeter of the rupture front, and in general is of order 1.

This formula for \dot{C} is very similar to that for \dot{W} , although in (26) the stress drop replaces the frictional stress appearing in equation (18) for \dot{W} . The initial impression, in comparing formulas for \dot{C} and \dot{W} , might therefore be that the work rate over the perimeter of a fault surface has about the same magnitude as work rate over the surface of the rupturing fault. However, it is shown below that this conclusion is untenable in view of the consequences of such a high value for \dot{C} . It follows that the stress drop is much less than the initial shear stress, or, more likely, the dimensionless factor at the end of expression (26) must be very small, thereby constraining the rupture velocity, or both.

To establish these several points, let us discuss the balance of work rates at the rupture front.

In part, the work rate is done against cohesive forces (summarized above as a surface energy with magnitude 1000 ergs/cm^2), and the remainder must generate heat as a moving line source located at the rupture front. The work rate against cohesion appears to be almost completely insignificant, since expected values would be the surface energy $\times v_n \times 2$ (accounting for both faces of the fault), yielding $6 \times 10^8 \text{ ergs/(cm sec)}$ if the rupture speed is 3 km/sec . After about $1/3 \text{ sec}$ of fault motion, when the fault radius is about 1 km , the total work rate against cohesion (i.e., all around the rupture front) is only about 10^{-8} of the work rate \dot{W} given in equation (18). The total work rate against cohesion (\propto circumference $\propto t$) is a higher fraction of the work rate $\dot{W} (\propto t^2)$ at earlier times, but the fraction is still only 10^{-5} when the fault radius is about 1 meter . This clearly establishes the insignificance of work in cohesion effects in comparison to large-scale friction phenomenon, but for a better appreciation we must compare cohesion effects directly with rupture front work rates. That is, we must ask how big $6 \times 10^8 \text{ ergs/(cm sec)}$ is, in comparison with \dot{D} , the work rate available in the elasticity solution, as given by equation (25). \dot{D} has considerable variation with position, in our elliptical crack solution, and the quantity $\dot{D}/(a^2 t)$ is shown for several choices of rupture velocities in Figure 5.

Apart from a few special positions for which \dot{D} is zero, it appears from the Figure 5 that typically $\dot{D}/(a^2 t)$ is of order $10^{10} \text{ ergs cm}^{-3}$. Therefore, with $a \sim 10 \text{ cm/sec}$, and t greater than $1/100 \text{ sec}$, \dot{D} appears to be more than 100 times greater than the work rate against cohesion. For rupture duration greater than 1 sec , \dot{D} is about 10^4 greater than the work rate against cohesion. Figure 5 also does show that \dot{D} is very sensitive to changes in rupture speed v_n , so that with only slight departures from an elliptical fault surface it might well be possible to reduce \dot{D} all around the rupture front, rather than in localized regions. The dilemma now confronting us is to decide whether \dot{D} must be of the order of $6 \times 10^8 \text{ ergs cm}^{-1} \text{ sec}^{-1}$, or whether it may be many orders of magnitude greater, with the excess (over work against cohesion) going into heat generated at the rupture front. The first alternative has been widely favored by theoreticians, ever since the pioneering work of Barenblatt. For the present problem, involving a three-dimensional solution, with rupture front oblique to the slip and the stress jump, it is shown below that a low value of \dot{D} implies the rupture speed must in general exceed the Rayleigh speed, and that energy must be extracted from the screw dislocation in the usual fashion, but is then used to drive the edge dislocation at a speed which absorbs the energy excess over that required to break new fault surface. The second alternative presents a very different picture, in which the underlying phenomenon of rapid fracture is intimately related to substantial thermal effects. Fuller *et al.* (1975) have measured a 500° temperature rise at the tip of fast-moving tension cracks in glassy polymers, and one would expect shear cracks to be associated with even greater heating effects. It thus appears that experiments to determine surface energy of fracture (whether in tension or in shear) need to be designed to observe associated thermal processes.

First alternative: a low value for rupture-front work rate. If \dot{D} (see equation 25) is to approximate the work done against cohesion, then the dimensionless expression

$$E(\phi) = [\mathcal{R}(v_n)N^4 \cos^2 \phi + B_s^2(v_n/\beta)^2 \Sigma^4 \sin^2 \phi]/B_s \quad (27)$$

must be of order 10^{-4} , about $1/100$ th of a second after rupture, and reduces to 10^{-6} , about 1 sec after rupture. Note that $E(\phi)$ is composed of terms which in general are of order one. The reciprocal variation with time is a property of our brittle fracture solution, with its stress intensity increasing as rupture progresses, and it appears inconsistent to discuss temporal variations in the value of $E(\phi)$, since the rupture speeds in our model do not change. However, from (15) and (16) we have pointed out fundamental ratios

between intensity factors for stress and particle velocity, enabling us to obtain a more general result for \dot{D} . Thus, if the relations

$$\tau_{zn}(n)^{1/2} \sim K(\phi, t)H(n)$$

$$\tau_{tz}(n)^{1/2} \sim L(\phi, t)H(n)$$

define the stress intensity factors for plane strain and antiplane strain motions around the rupture, it follows that

$$\dot{D} = [2\pi\mu\beta^2/(\alpha v_n^2)][\mathcal{R}(v_n)K^2 + \frac{1}{4}B_s^2(v_n/\beta)^2L^2]/B_s. \quad (28)$$

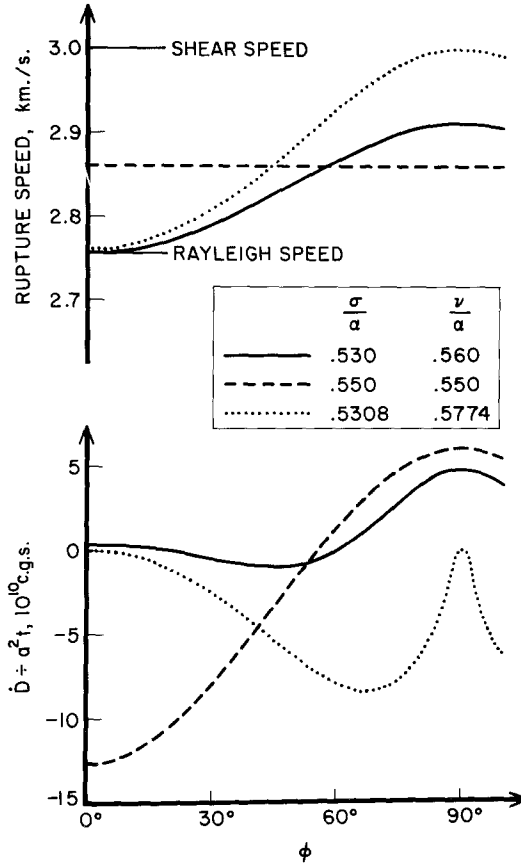


FIG. 5. Diagrams to show the sensitivity of work rate to slight changes in rupture speed. For three different choices of the rupture parameters σ and ν , the local variation of rupture speed v_n with azimuth ϕ is shown in the upper part of the figure. Below are shown corresponding values of the work rate \dot{D}/a^2t , for the medium such that $\alpha = 5.2$ km/sec, $\beta = 3$ km/sec, $\rho = 2.7$ gm/cc. The dotted line is for the case $\sigma =$ Rayleigh-wave speed, $\nu =$ shear speed. \dot{D} is then zero at $\phi = 0^\circ$ and $\phi = 90^\circ$. Very low values of \dot{D} are given by the solid line, for the range $\phi = 0^\circ$ to $\phi = 60^\circ$.

This relation is similar to a result obtained by Kostrov and Nikitin (1970).

The main point to make about both formulas (27) and (28) is that the terms involving $\mathcal{R}(v_n)$ and B_s^2 must substantially cancel each other out, if \dot{D} is to be of the order of the work rate against cohesion only. Thus, the quantity $\mathcal{R}(v_n)$ must be negative, which requires v_n to exceed the Rayleigh-wave speed. The negative value for $\mathcal{R}(v_n) K^2$ in (28) can be interpreted physically as a negative work rate performed by the plane strain component of motion—a component which must be driven by the (positive) work rate of the anti-

plane strain component. Burridge (1973) has pointed out that super-Rayleigh rupture speeds are unphysical, when they imply that the rupture front is a net energy source which radiates motion into the surrounding medium. This would occur, for example, in a two-dimensional problem with plane strain throughout the medium, and a rupture front moving as a straight line with speed higher than the Rayleigh speed. In our three-dimensional geometry, however, rupture speeds lying between the Rayleigh speed and the shear-wave speed are perfectly acceptable. From the point of view of the surrounding medium, the rupture front acts as a substantial sink for antiplane strain motions, and a substantial (slightly smaller) source for plane strain motions. The net effect is still that of a sink, and the energy thus lost from the medium is used at the rupture front to do work against (i.e., to “break”) cohesive bonds.

Second alternative: a high value for rupture front work rate. If the two terms in (27) for $E(\phi)$ do not effectively cancel, then \dot{D} will be large, and the total work rate around the rupture front (\dot{C}) could be of the same order as the frictional work rate over the fault surface (\dot{W}). The latter rate was found above to generate significant increases in temperature, so the spatially more concentrated heat source \dot{C} might be expected to generate even greater thermal effects.

To assess the moving line-source heating effect of the rupture front, it is instructive to solve the temperature diffusion equation (19), in which the heat source term is taken as all of the available work in the elasticity solution, i.e.,

$$A(\mathbf{x}, t) = \dot{D}\delta(n)\delta(z) \quad (29)$$

where \dot{D} is given by equation (25) and n measures distance normally from the moving rupture. Clearly, the variability of \dot{D} around the perimeter of an elliptical fault renders this problem insoluble in closed form. To obtain local temperature effects on the fault surface, in the vicinity of the curved-line source as it passes by, it is probably adequate to work with a straight-line source having a constant strength which locally is the same as (29). That is, we must consider the temperature solution for heat source

$$A(\mathbf{x}, t) = B\delta(x-vt)\delta(z) \quad (30)$$

in which the constant B is subsequently assigned values equal to \dot{D} . For convenience, we have here taken a line of heating parallel to the y axis, and propagating in the direction of increasing x . The solution of (19) with source (30) is, on the fault surface,

$$T = T(x, t) \Big|_{z=0} = \frac{B}{2\pi K} \exp [(-v/2\kappa)(x-vt)] K_0 \left(\frac{v}{2\kappa} |x-vt| \right) \quad (31)$$

in which K is the conductivity, κ the diffusivity, and K_0 is the modified Bessel function with logarithmic singularity $K_0(X) \sim -\ln X$ as $X \rightarrow 0$. This solution is shown in Figure 6, and we note that a logarithmic singularity is weak, compared to the type of singularity present in the stress field at the rupture front. The spatial scale for our temperature is discussed in the caption to Figure 6, and clearly the singularity is removable by spreading the heat source throughout a finite (but small) region around the rupture front. An adequate approximation to (31), valid even down to millimeter distances behind the rupture, is then given by

$$T = \frac{\dot{D}}{2\pi K} \left[\frac{\pi}{2(vt-x)} \right]^{1/2} H(vt-x). \quad (32)$$

The local heat production rate, \dot{D} , has been substituted here, together with the far-field approximation to K_0 , and we are now able to give order-of-magnitude estimates of the

heating effect at the rupture front. Taking from Figure 5 the value $\dot{D} \sim 10^{12} \times t$ ergs $\text{cm}^{-1} \text{sec}^{-1}$, and $K \sim 2 \times 10^5$ ergs $\text{cm}^{-1} \text{sec}^{-1}$ per $^\circ\text{C}$, we reach the following conclusions: for times about 1/100 sec after rupture, temperatures are raised at least 1000° throughout a strip of fault surface one meter in width, behind the rupture front. For times about 1 sec after rupture, temperatures are raised over 1000° for a strip of 10-km width. That is, the whole rupture surface must melt.

We have made several strong assumptions to reach this conclusion (the poorest being that into solution (31) we can replace the constant B by a local value of \dot{D} , when in fact \dot{D} is proportional to time). Nevertheless, it appears that temperatures are far too high unless the rupture front work rate \dot{D} is substantially less than that generally found in equation (25) for the self-similar elliptical fault. \dot{D} grows steadily with time, rapidly becoming much too large, except for special directions ϕ for which \dot{D} is zero (see Figure 5). These special directions are determined by finding zeros of the dimensionless expression $E(\phi)$ (see equation 27). However, it is found in practice that for any direction ϕ there is just

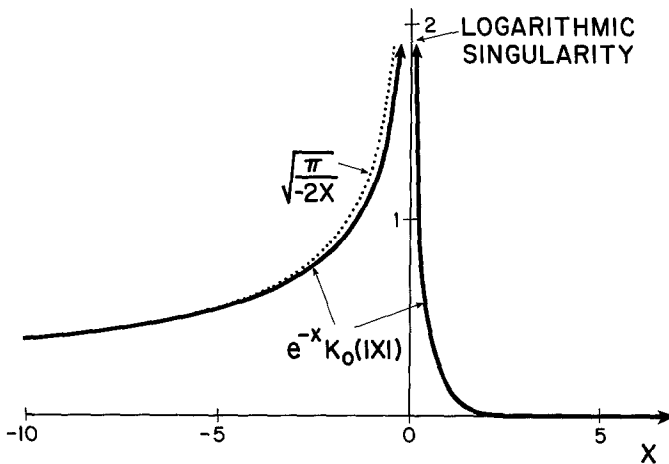


FIG. 6. Temperature effect near a propagating line heat source. The dimensionless variable X is $v(x-vt)/2\kappa$ (see equation 31), so $X = 1$ corresponds to a distance about 5×10^{-2} cm from the rupture. The vertical axis gives $2\pi KT/\dot{D}$ (see equation 31), so it is apparent from the figure that temperatures are elevated behind the moving rupture. At all distances of practical interest, the asymptotic equation (32) is adequate.

one value of rupture speed v_n in the range $\gamma \leq v_n \leq \beta$ for which $E(\phi)$, and hence \dot{D} , is zero, so that only small departures from the self-similar (elliptical) shape are necessary to make \dot{D} as small as may be desired. Although it might be satisfying to find an exact model, the inhomogeneities present in any given seismic region (inhomogeneities in initial stress, and in material properties) would hardly make it more useful than the elliptical model, for which a complete solution of the associated motions is available.

From this discussion of the thermal effects, we then conclude that \dot{D} cannot be as large as equation (25) indicates might be possible. It again follows that there must be some cancellation of the work rates in plane strain and antiplane strain, although the cancellation does not have to be so complete as was indicated above in the discussion of a balance with work done against cohesion only.

QUANTITATIVE DESCRIPTION OF MOTIONS NEAR A RUPTURING FAULT

In this section, detailed results are given for the self-similar elliptical crack, to obtain insight into the behavior of shear stresses and accelerations in the vicinity of a propagating

fault. Attention is concentrated on points near the fault plane, since we are interested in trying to detect the presence of rupture as it moves past observing stations: many of the computations are carried out for the case $\theta = 85^\circ$.

Figure 7 shows one of the quantities which can easily be computed. At the *lower left side* is shown a quadrant of the elliptical part of the fault, which is in motion. In this case, rupture in the x direction is taken as the Rayleigh speed, and in the y direction as the shear-wave speed. The xz component of stress is being relieved by the fault, and the major part of Figure 7 shows four different time histories for the stress rate $\dot{\tau}_{xz}$, at different azimuthal angles ϕ , for points near the fault plane. It is the stress rate which comes naturally out of the solution method, and it is natural to express the solution in a dimensionless form. The factors relating dimensionless and dimensioned stress rates and

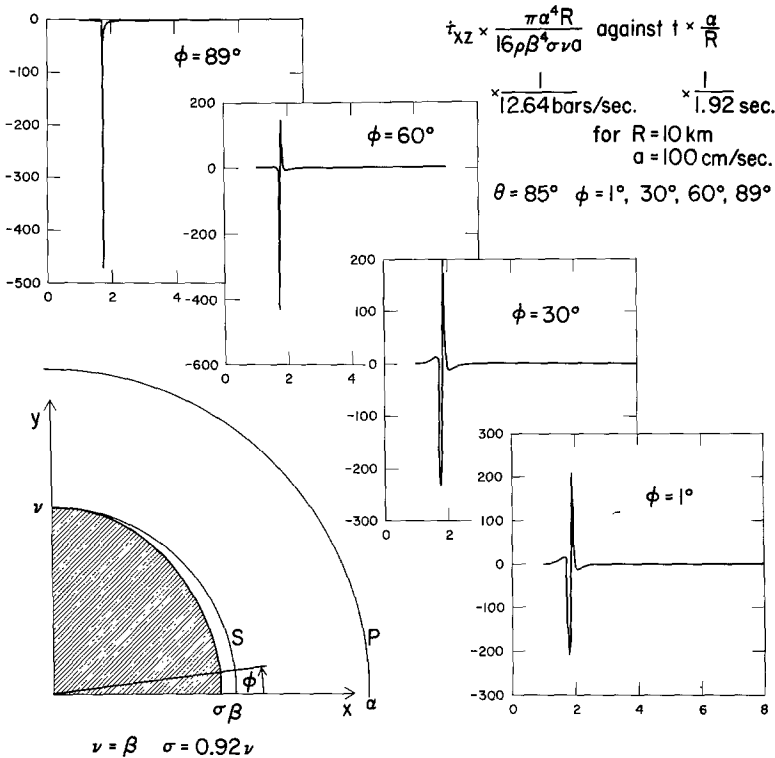


FIG. 7. The time history of stress rate, shown at four different azimuths. At the *bottom left side* is shown a quadrant of that part of the fault surface which is in motion (shown shaded), giving relative positions of the S wave front and the P wave front. Stress rate and time are plotted as dimensionless quantities, and factors shown at the *upper right side* may be used to convert the plots to dimensioned values for specific cases. Density and wave speeds are the same as for Figure 5.

times are shown at the *upper right side* of Figure 7. Particular values of these dimensioning factors are shown, for a point 10 km away from the initial rupture, with an assumed particle velocity of 100 cm/sec for the initial rupture. At azimuth $\phi = 0^\circ$, the medium is in a state of plane strain, and is in antiplane strain at $\phi = 90^\circ$. These particular values are replaced by $\phi = 1^\circ$ and $\phi = 89^\circ$ in computations, to avoid divisions by zero in the present program. Since computed solutions for $\phi = \frac{1}{2}^\circ$, $\phi = 1^\circ$, $\phi = 2^\circ$ are found to be the same for all practical purposes, as are the solutions for $\phi = 88^\circ, 89^\circ, 89\frac{1}{2}^\circ$, the output for $\phi = 1^\circ$ can indeed be taken as representing plane strain, and $\phi = 89^\circ$ as antiplane strain.

Figure 8 shows the result of time-integrating Figure 7, to obtain τ_{xz} itself. Again, the shear stress is plotted in dimensionless form for four points near the fault plane, differing

only in azimuthal angle. It may be seen that τ_{xz} has a rather different time history at each of the four azimuths, but the value for large times is everywhere the same, about -8 units. With an initial particle velocity of 100 cm/sec, this translates to a stress drop of about 200 bars. Figure 9 differs from Figure 8 only in that the rupture velocities are halved. For the same initial particle velocity of 100 cm/sec, the stress drop now is about 300 bars.

We should like to emphasize the three-dimensional nature of this earthquake model. Because the xz component of stress is the only component being relieved by fault motion, it follows that the other shear component on the fault plane, τ_{yz} , should have final values unchanged from zero. Figure 10 shows this indeed to be the case, in that τ_{yz} at different positions near the fault plane does tend to zero for large times, but it will be seen at intermediate values, particularly at times near the rupture arrival, to be large. This kind

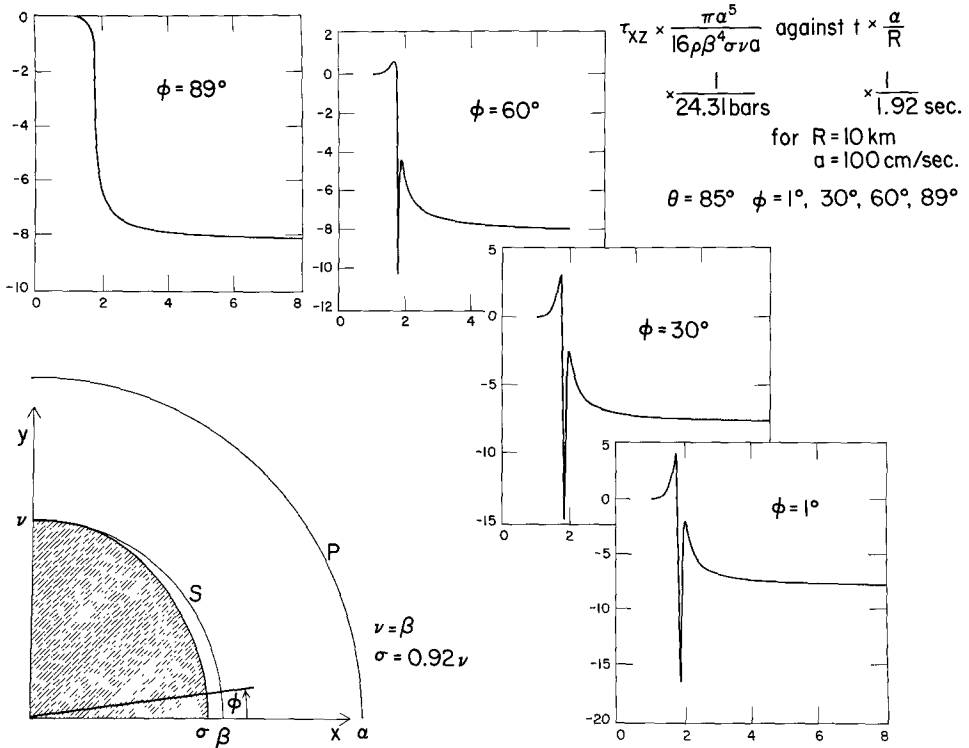


FIG. 8. Same as Figure 7 but showing stress. This figure was obtained via a time integration of Figure 7.

of feature is important to consider, since fault motions must begin at a point, and then spread over the fault surface with a rupture front which is a closed curve (or several closed curves) in the fault plane.

Figures 7, 8, 9 and 10 all describe the stress history near a rupturing fault and help us to understand how stress is relieved by the stress relaxation phenomenon of the earthquake. But, of course, seismic instruments are built typically to record acceleration, or displacement. Figure 11 shows both, again for four different azimuths. Plotted here as solid lines are the x components of acceleration. The dashed lines are corresponding displacements, and the dotted line is the displacement time history for that point on the fault surface which is nearest the station with azimuthal angle as shown, and $\theta = 85^\circ$. Acceleration clearly has a different time history at these locations, and if particle velocity is 100 cm/sec on the fault, then maximum accelerations are around 1 g at the distance

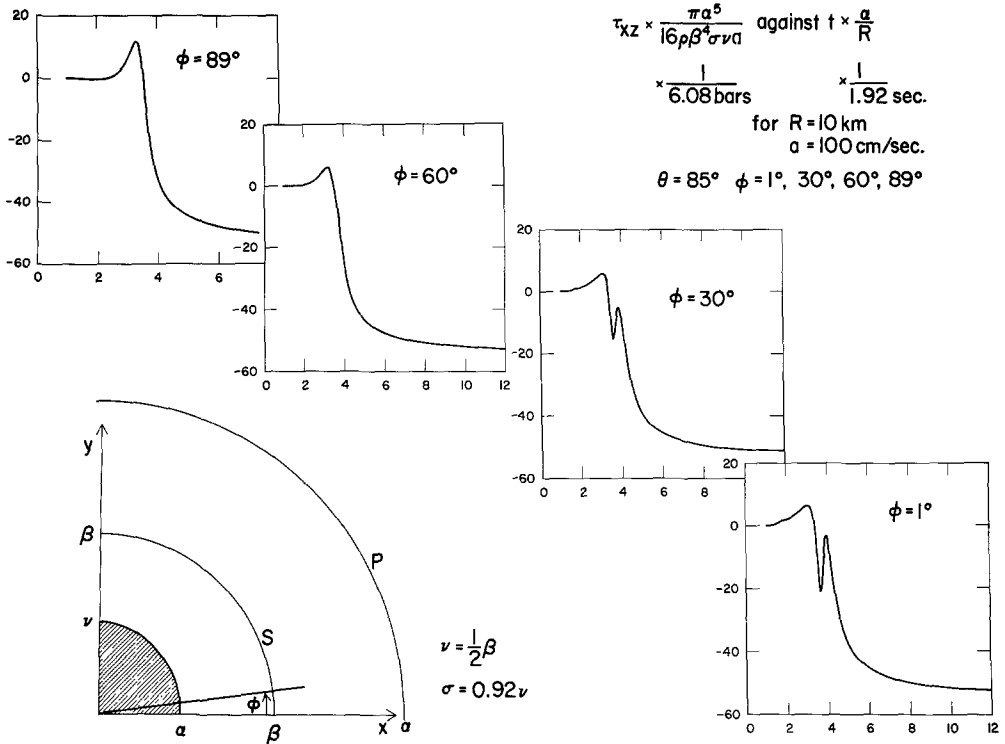


FIG. 9. Same as Figure 8, but with rupture speeds halved.

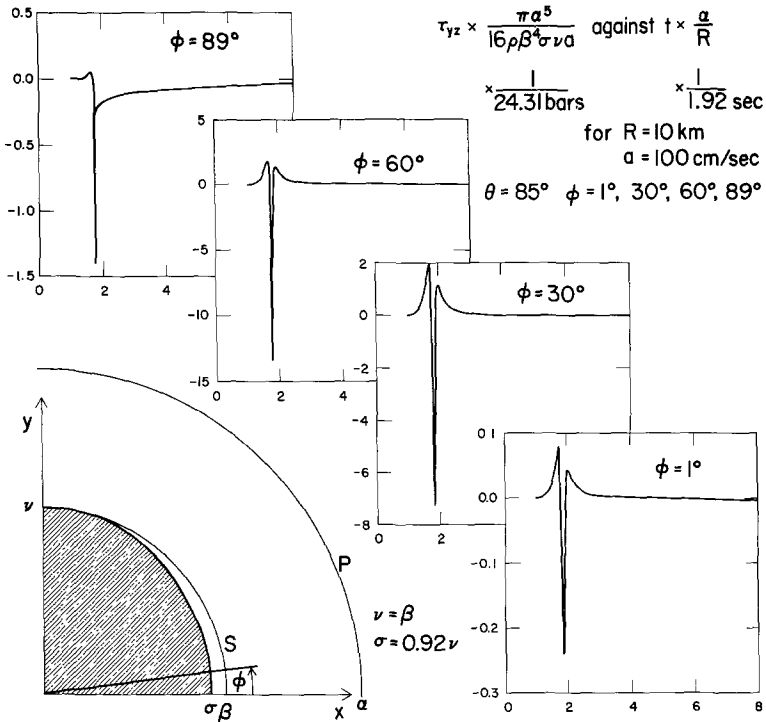


FIG. 10. Same as Figure 8, but for the τ_{yz} component of shear.

10 km, for $\phi = 1^\circ, 30^\circ$ and 60° . The case $\phi = 89^\circ$ is pathological, because the rupture is essentially riding on the S wave front, and accelerations are up to around several tens of g , due to the focusing of energy. However, the displacement (obtained by double integration of acceleration) is about the same at all four different positions, and in each case the computed displacement (shown dashed) is similar to the dotted curve, the actual shear slip of the nearest point on the fault surface (obtained from equation 4).

Another displacement that is important to investigate is the component normal to the fault plane. Figure 12 shows the acceleration and displacement in this direction, in the case of slow rupture propagation. The first remarkable point is that the acceleration time history has essentially the same shape at all four stations. However, the scale is very different. This similarity in shape is due to the fact that that part of the fault plane which is in motion has been twisted through a constant angle out of its original plane,

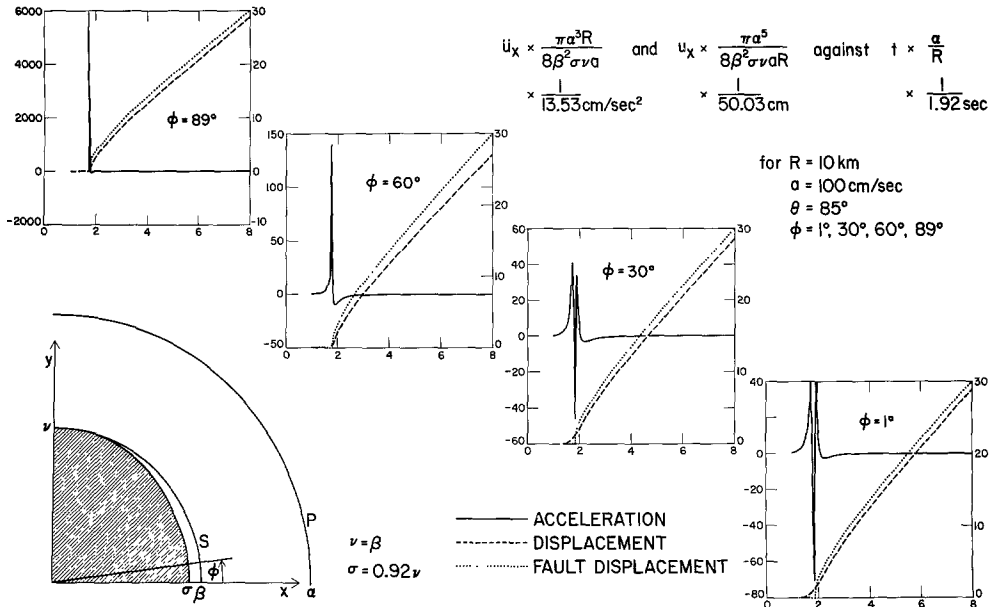


FIG. 11. Same as Figure 7, but showing the x -component of acceleration and displacement. Acceleration values are obtained from the solid curves, and left-hand vertical scales: displacements from the dashed curves, and right-hand scales. Dotted curves show the displacement time history at nearest points on the fault surface itself.

so that the z components of acceleration and displacement have a magnitude which is proportional to the x coordinate. Displacement is shown here as a dashed line. The second important point to make is that the z displacement may be a good marker of the rupture front going nearby. If one actually had data for displacement of the type shown as dashed lines in Figure 12, then one would not be far wrong in picking the times of rapid change in z displacement as the time the rupture front is passing nearby.

The problem of obtaining the rupture speed, from a record section obtained along the fault plane, is met with in practice both in seismology and in the more controlled circumstances of rock mechanics experiments. That there is a problem is demonstrated by Figure 13, showing a theoretical record section of accelerations (using the elliptical crack) for which the rupture speed is known to be less than the shear-wave speed, but apparently indicating a faster rupture speed. The geometry of the array of four transducers (see Figure caption for details) is such that we may regard this as a plane strain problem, to study motions near a left-lateral strike-slip fault. The *top* of Figure 13 shows

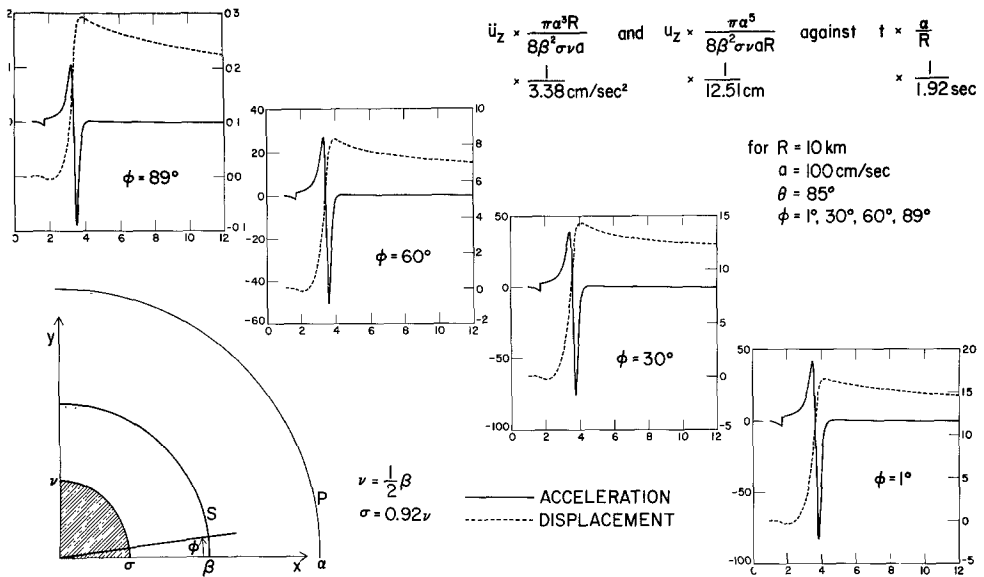


FIG. 12. Same as Figure 11, but for the slower rupture speeds, and the z-component of acceleration (solid) and displacement (dashed).

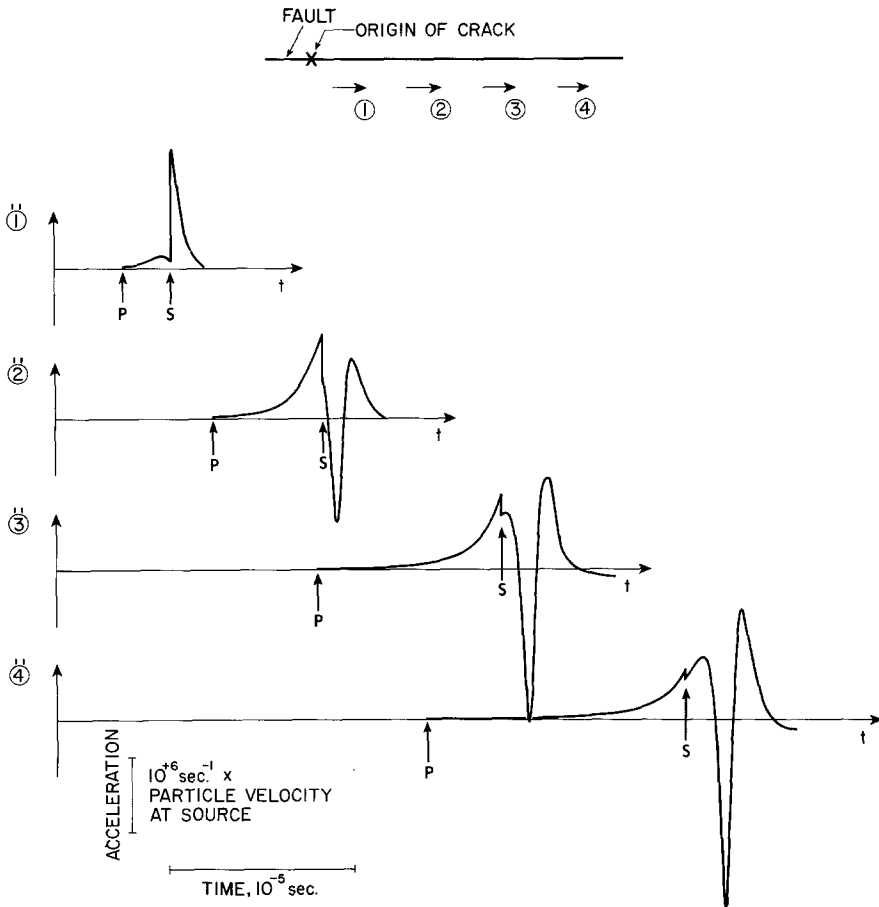


FIG. 13. A theoretical record section for accelerations in a rock mechanics experiment. Receivers 1, 2, 3 and 4 are at (x, y, z) coordinates given, respectively, by $(1, 1.5, 0.5)$, $(4, 1.5, 0.5)$, $(7, 1.5, 0.5)$, $(10, 1.5, 0.5)$ cm. That is, they are spaced 3 cm apart. We may imagine them placed on the surface of a 3-cm plate of the rock sample ($\alpha = 5.1 \text{ km/sec}$, $\beta = 3 \text{ km/sec}$) and $\frac{1}{2}$ cm from a pre-cut friction surface (fault). Rupture nucleates at $(0, 0, 0)$ within the sample, and the section shown is for $\sigma = 2.8 \text{ km/sec}$, $\nu = 2.9 \text{ km/sec}$. Even though the rupture is nearest each station at times *after* the S arrival, considerable acceleration is apparent *prior* to S, in the tail of the P wave, and might naively be picked to mark the rupture.

a map view of the fault, and depth is in the direction of negative y . The transducers are placed at distances 1, 4, 7 and 10 cm along the fault (measured from the point of nucleation), but are all $\frac{1}{2}$ cm away from the fault surface itself. Since they measure motions in the x direction, the predicted records will be similar to the known fault surface motions (equation 4), for which P - and S -wave arrivals are absent. However, due to their physical size, the transducers must be placed a slight distance away from the fault. Figure 13 shows that computed P arrivals are insignificant at the four stations, and that S arrivals get less significant with increasing distance. In fact, the rupture speed is

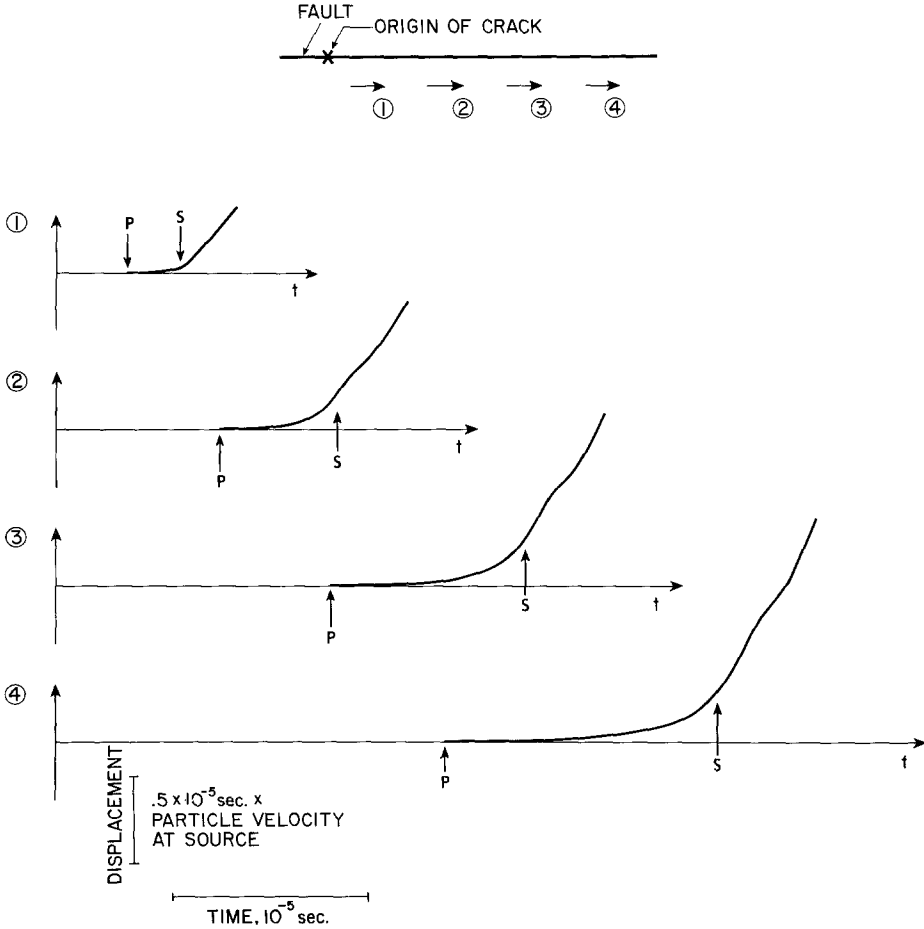


FIG. 14. Same as Figure 13, but now showing displacements.

about 7 per cent less than the S -wave speed, yet one might naively pick times (for the rupture going nearby) which are near the S -wave arrival, even preceding this arrival at the farther stations (transducers), and hence obtaining an estimate for the rupture speed which is greater than the S -wave speed.

If these acceleration records are integrated twice, the displacement record is as shown in Figure 14. The presence of the rupture front is, in Figure 13, associated with rapid fluctuation in acceleration, but in Figure 14 the corresponding effect is almost unnoticeable, being only a change in curvature. If displacement records like those of Figure 14 were obtained in an experiment, it would clearly be futile to try to use them for accurate estimation of the rupture speed. The experiments reported by Johnson *et al.* (1973) used

strain transducers, oriented to record the component e_{xx} , and Figure 15 shows one of their observations. A theoretical record for one of these strain observations, using the elliptical crack, is given in Figure 16, showing again that substantial strain is present just before the S -wave arrival, even though strains local to the rupture front would arrive later than the S wave. These rupture strains occur near the time marked as R in Figure 16.

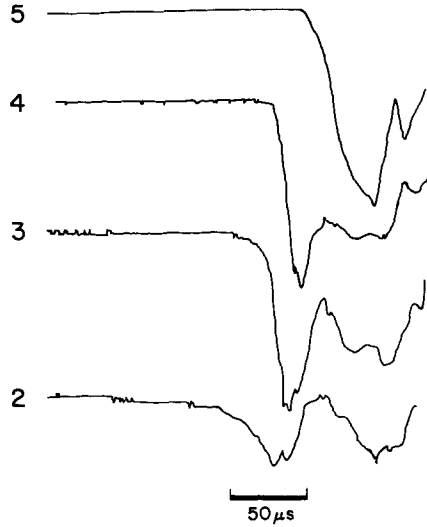


FIG. 15. An observational record section for the strain component e_{xx} , obtained for a stick-slip event in Westerly granite. See Johnson *et al.* (1973) for details. Transducers 2 and 3, and 3 and 4, are about 2.4 cm apart. Transducers 4 and 5 are about 4 cm apart. Other coordinates are the same as for the stations in Figure 13. The interpretation is of rupture propagating rapidly past stations 2, 3 and 4, with some slowing down between 4 and 5.

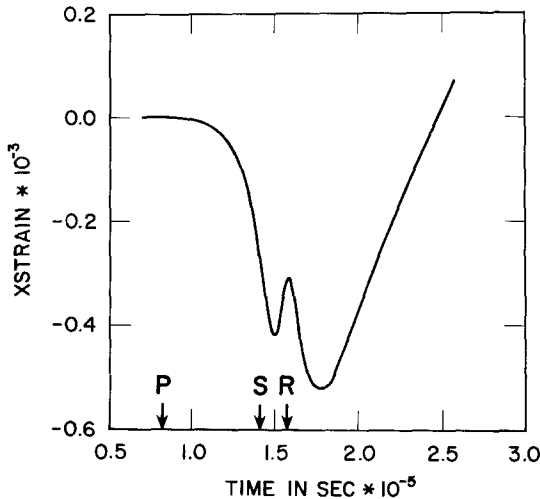


FIG. 16. A theoretical record for e_{xx} strain, using the elliptical crack with particle velocity $a = 100$ cm calculated for a station with coordinates (4, 1.5, 0.5) cm. The rupture speed here is 90 per cent of the shear-wave speed.

The possibility of using motions normal to the fault surface to infer the rupture speed was mentioned above in connection with Figure 12. This possibility is explored further in Figure 17, in which record sections are given for both \ddot{u}_x and \ddot{u}_z accelerations near a left-lateral strike-slip fault. These components are commonly referred to as “parallel” and

“transverse” components, respectively. Figure 17 shows that the transverse component is the larger, although it does not appear to be more effective than the parallel component in showing any particular marker for the rupture front passing nearby. Two integrations of these accelerations yield the displacement records shown in Figure 18, and give a very different comparison between transverse and parallel components. The transverse displacement is now the smaller (it tends to a constant, and the parallel component grows without limit in the self-similar solution), and is much better as a marker of the rupture

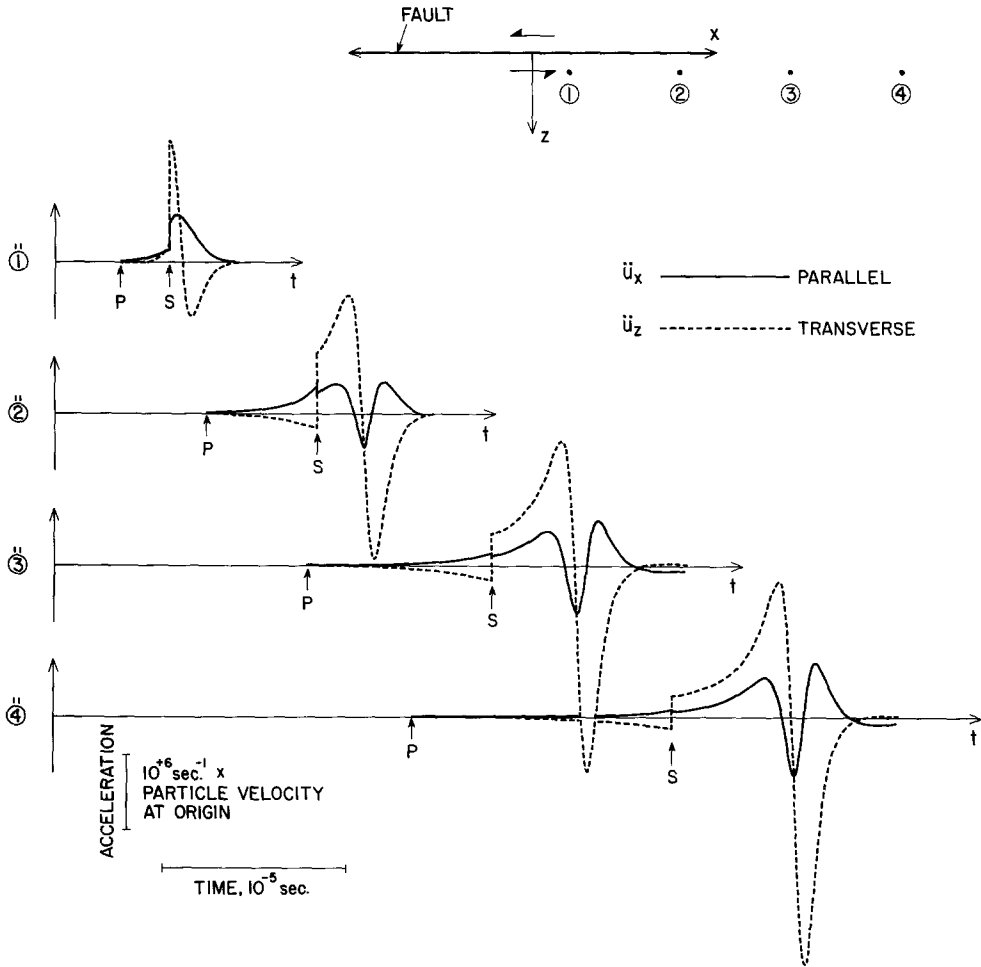


FIG. 17. Theoretical record sections for x and z components of acceleration near a left-lateral strike-slip fault. Coordinates for the four stations are the same as Figure 13. Here, the density and wave speeds for P and S are the same as for Figure 5. Rupture speed in the x direction is 90 per cent of the Rayleigh-wave speed.

front. Figure 18 clearly suggests that more attention should be paid to using the transverse component in rock mechanics experiments, although the parallel displacement may “blur” the more sharply rising transverse displacement, if the observations are carried out on a free surface (which itself involves boundary conditions which may link the two components of motion). Archuleta and Brune (1975) have studied components in a foam rubber model and obtained qualitative confirmation of several predictions of the elliptical crack solution. In particular, they found that particle velocities near a fault surface increase with distance from the point of nucleation along the fault, as would be expected from

examination of points A, B, C in Figure 3 of this paper. Much of Archuleta and Brune's (1975) observations concern end effects (stopping effects) and so cannot be compared to a dynamic self-similar solution. Before such effects become apparent, however, the comparison is possible and useful, although in their experiment Archuleta and Brune (1975) had no basis for knowing one of the two rupture velocities in the self-similar elliptical model. They have been able to get a good estimate of the static stress drop, but not of the dynamic stress drop, and it is the latter which is needed to scale the self-similar solution, as we next discuss.

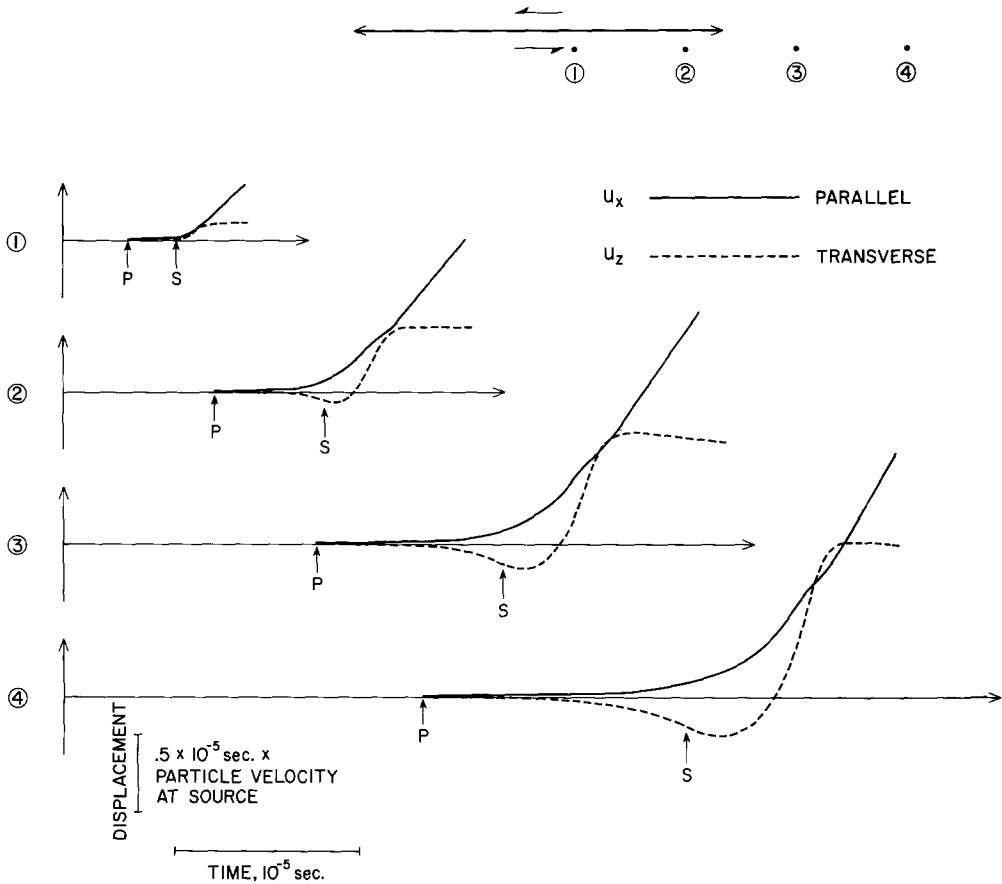


FIG. 18. Same as Figure 17, but showing displacement.

RELATIONSHIP BETWEEN STRESS DROP AND PARTICLE VELOCITY AND DISCUSSION OF OVERSHOOT

The stress relaxation model being described in this paper has the property of a dynamic stress drop (i.e., minus τ_{zx} on the moving part of the fault surface) which is proportional to particle velocity at the initial point of rupture (Burrige and Willis, 1969). It is clearly useful to know the constant of proportionality, and in Figure 19a is plotted a value for this constant, for a range of rupture velocities. The solid curve in Figure 19a was obtained by evaluating an integral given by Kostrov (1964), for a circular crack. Dahlen (1974) gives an equivalent integral, and the user should be aware that the formulas of both authors contain clear typographical errors. Another way to get Figure 19a is to take the time history of stress rate as shown in Figure 7 for a point near the fault plane, and to

integrate this up to find the final value (which in the self-similar solution is the dynamic value) of the stress drop. Carrying this procedure out at the rupture speeds used for Figures 8 and 9 results in the two crosses shown in Figure 19b. (These computations are for an elliptical crack which is nearly circular: the average value of rupture velocity was used to plot the crosses.) The agreement of the crosses with Kostrov's curve gives one confidence that the extensive numerical work, since it is self-consistent, is correct.

Brune (1970) has discussed the radiation from a stress pulse which is suddenly applied throughout the entire fault plane ($z = 0$). This corresponds to infinite rupture velocity and may be considered a one-dimension problem, since motion is dependent spatially

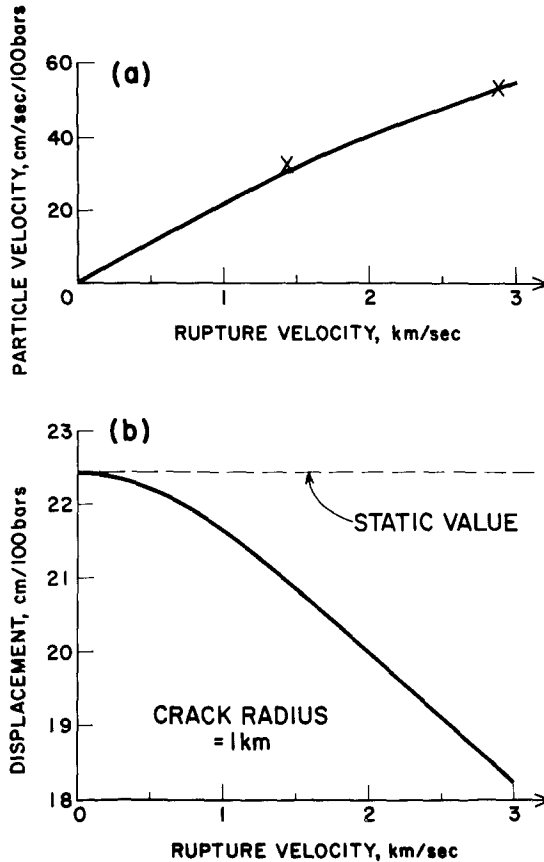


FIG. 19. (a) Evaluation of formulas given by Kostrov (1964) for the particle velocity at fixed stress drop, shown as a function of rupture speed, for a circular shear crack. Two crosses mark the values derived from Figures 8 and 9. (b) Fault displacement (i.e., half the maximum offset), shown as a function of rupture speed, at the time the fault acquires a radius of 1 km.

only on the z coordinate. He finds that particle velocity is given by $\beta\tau_{zx}/\mu$ for stress jump τ_{zx} , and if this is 100 bars, the particle velocity is 123 cm/sec for the medium considered in Figure 19a. This value is about twice that of the highest particle velocity shown for subsonic rupture. Note, however, that by "particle velocity" in Figure 19a, we mean the constant "a" of equation (4), which is the asymptotic value as time increases. Figure 3 shows that particle velocity is singular at the rupture front and rapidly decreases to the asymptotic value.

The basic observation to make about Figure 19a is that the curve is almost a straight line through the origin. However, the slight negative curvature is important, since it

implies that faults are unlikely significantly to overshoot their final static displacement. One can conclude this by comparing the displacement offset in the dynamic self-similar solution, at the particular time for which the crack has reached a given size, with the offset in a static solution for a crack of the same size. For example, the size in question is a circular fault of radius r . The dynamic offset is (from equation 4)

$$[u_x] = 2a(t^2 - x^2/v^2 - y^2/v^2)^{1/2} \quad (33)$$

on the crack, where we have taken speeds σ and v both equal to v . Equation (33) may be rewritten for the displacement on $z = 0^+$ as

$$u_x = at \{1 - x^2/(v^2 t^2) - y^2/(v^2 t^2)\}^{1/2} \quad (34)$$

and this gives a static distribution in the limit as $a \rightarrow 0$, $v \rightarrow 0$, $t \rightarrow \infty$, such that $vt = r$ and $2at =$ offset at the center. Eshelby (1957) has given the relation between stress drop τ_{zx} and offset for static elliptical cracks, and his results for the circular crack of radius r can simply be stated in terms of the displacements on the surface $z = 0^+$

$$\begin{aligned} u_x &= \frac{r\tau_{zx}}{\mu} \cdot \frac{4\alpha^2}{\pi(3\alpha^2 - 2\beta^2)} \cdot \left(1 - \frac{x^2 + y^2}{r^2}\right)^{1/2} \\ u_y &= 0 \\ u_z &= \frac{x\tau_{zx}}{\mu} \cdot \left(\frac{\beta^2}{3\alpha^2 - 2\beta^2}\right) \end{aligned} \quad (35)$$

Note the familiar features that u_x is elliptical in space, that slip is only in the x direction, and that u_z is proportional to x .

It is clear from (34) that the displacement (of each side of the crack) at the center ($x = y = 0$) is $a \times r/v$, at the time the crack reaches radius r . This displacement is shown as the curve in Figure 19b, obtained for a crack radius of 1 km by dividing the curve of Figure 19a by the rupture velocity. The dashed line in Figure 19b is the displacement u_x from equations (35) (with stress drop 100 bars), and it is gratifying to find that the dynamic solution in the limit of zero rupture velocity does agree with Eshelby's static solution: both displacements are 22.4 cm.

If we suppose that the dynamic self-similar solution is valid during growth up to a crack radius of 1 km, but that then the rupture were to stop, we ask: "Would displacement across the fault continue to grow in the same direction, or would it have to reverse?" The curve shown in Figure 19b is everywhere (for nonzero rupture speed) below the static level, so that if the fault displacements are to end up in a final static configuration which is appropriate to the same stress drop as that prevailing during rupture, the displacement will have to grow up to the static value from below, and overshooting will not be required, although of course it still may be possible. If the dynamic curve in Figure 19b were above the static curve, then overshoot would be necessary. This problem, for a circular crack, is currently being studied by Madariaga (1975). A detailed solution has been published by Burridge (1969, see his Figure 16) for the corresponding plane strain two-dimensional problem of a growing slit of infinite extent, and he finds (for a rupture speed equal to half the P -wave velocity) that slight overshoot does occur. We show in Figure 20a the two-dimensional analog of Figure 19a, using another integral of Kostrov (1964) for the proportional constant relating particle velocity and stress drop in the case of a growing slit, and in Figure 20b the central displacement for a slit half-width of 1-km is plotted against rupture speed. This Figure indicates a much greater difference, between the dynamic and static displacements, in the two-dimensional model than for the three-dimensional model (shown by light lines in Figure 20b). If this can be taken to

indicate that, at all times, the dynamic displacements on the fault surface in three dimensions are more like the corresponding static solution than is the case in two dimensions, then the small overshoot known to occur in two dimensions would indicate an even smaller overshoot in three dimensions. However, the actual situation is more complicated by the fact that the dynamic stress drop prevailing during rupture may well be greater than the final value, i.e., the static value attained after all motion has ceased. Clearly, this would reduce the static offset below the static offset we have been discussing in connection with Figures 19b and 20b (since the offset is proportional to stress drop),

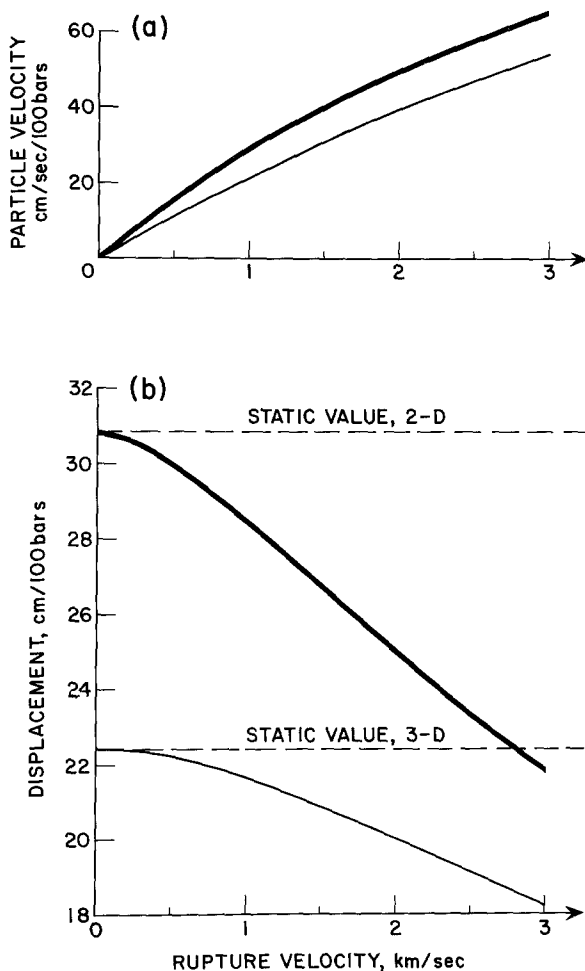


FIG. 20. Same as Figure 19, but for the two-dimensional plane strain problem of a growing strip. The heavy lines are the two-dimensional solution; light lines are from Figure 19, i.e., three dimensions, for comparison. In (b), the slit half-width is 1 km.

making overshoot more likely than we would have supposed. Further discussion of this problem must depend heavily on the physical processes by which rupture is stopped in space and time.

CONCLUSIONS

In studying the motions and stress changes which occur during the rupture process of an earthquake, one can be considerably assisted by the known solution for the dynamic field of a growing plane elliptical shear crack.

In this earthquake model, fault motions are presumed to nucleate at a point in an infinite pre-stressed elastic medium, and the rupture subsequently grows steadily with subsonic speeds, maintaining the shape of an ellipse. Shear stresses are relieved by the fault, dropping (on the fault surface) to the normal stress times the coefficient of dynamic friction.

Since displacements and stresses can readily be calculated everywhere for this three-dimensional model, we have used it to study heat generation and temperature rise, to obtain likely values for the rupture speeds, and to see how particle velocity and stress drop are related. Temperatures are found to rise considerably, even to melting on the fault surface. Rupture speeds are found to lie between the Rayleigh-wave and shear-wave speeds, and excess energy available from the antiplane component of motion is used to drive the plane strain component at speeds greater than would have been expected from a knowledge of two-dimensional solutions. The particle velocity is found to be, at most, half the value suggested by Brune (1970), and a comparison of dynamic and static solutions suggests that significant overshoot does not occur.

ACKNOWLEDGMENTS

I thank Dr. Tracy Johnson for contributing Figures 15 and 16, and Profs. Scholz and Sykes for their critical reviews. This research was supported by the Advanced Research Projects Agency of the Department of Defense, and was monitored by the Air Force Office of Scientific Research under Contract F44620-74-C-0029.

REFERENCES

- Achenbach, J. D. (1974). Dynamic effects in brittle fracture, in *Mechanics Today*, vol. 1, S. Nemat-Nasser, Editor, Pergamon Press, New York.
- Achenbach, J. D. and A. M. Abo-Zena (1973). Analysis of the dynamics of strike slip faulting, *J. Geophys. Res.* **78**, 866–875.
- Aki, K. (1968). Seismic displacements near a fault, *J. Geophys. Res.* **73**, 5359–5376.
- Anderson, J. G. and P. G. Richards (1975). Comparison of strong ground motion for several dislocation models, accepted for publication, *Geophys. J.* (in press).
- Archuleta, R. J. and J. N. Brune (1975). Surface strong motion associated with a stick-slip event in a foam rubber model of earthquakes, *Bull. Seism. Soc. Am.* **65**, 1059–1071.
- Brace, W. F. and J. B. Walsh (1962). Some direct measurements of the surface energy of quartz and orthoclase, *Am. Mineralogist* **47**, 1111–1122.
- Broberg, K. B. (1960). The propagation of a brittle crack, *Arkiv För Fysik* **18**, 159–192.
- Brune, J. N. (1970). Tectonic stress and the spectra of seismic shear waves from earthquakes, *J. Geophys. Res.* **75**, 4997–5009.
- Burridge, R. (1968). Theoretical seismic sources and propagating brittle cracks, *J. Phys. Earth* **16**, 83–92.
- Burridge, R. (1969). The numerical solution of certain integral equations with non-integrable kernels arising in the theory of crack propagation and elastic wave diffraction, *Phil. Trans. Roy. Soc., London, Ser. A* **265**, 353–381.
- Burridge, R. (1973). Admissible speeds for plane-strain self-similar shear crack with friction but lacking cohesion, *Geophys. J.* **35**, 439–455.
- Burridge, R. and L. Knopoff (1964). Body force equivalents for seismic dislocations, *Bull. Seism. Soc. Am.* **54**, 1875–1888.
- Burridge, R. and J. R. Willis (1969). The self-similar problem of the expanding elliptical crack in an anisotropic solid, *Proc. Camb. Phil. Soc.* **66**, 443–468.
- Dahlen, F. A. (1974). On the ratio of *P*-wave to *S*-wave corner frequencies for shallow earthquake sources, *Bull. Seism. Soc. Am.* **64**, 1159–1180.
- Davies, D. and A. M. Ziolkowski (1971). Size of earthquakes, in *Lincoln Laboratory Semiannual Technical Summary, Seismic Discrimination*, 31 Dec.
- Douglas, A., J. A. Hudson, P. D. Marshall, and J. B. Young (1974). Earthquakes that look like explosions, *Geophys. J.* **36**, 227–233.

- Eshelby, J. D. (1957). The determination of the elastic field of an ellipsoidal inclusion, and related problems, *Proc. Roy. Soc. London* **241**, 376–396.
- Fuller, K. N. G., P. G. Fox, and J. E. Field (1975). The temperature rise at the tip of fast-moving cracks in glassy polymers, *Proc. Roy. Soc. (London), Ser. A* **341**, 537–557.
- Gakenheimer, D. C. and J. Miklowitz (1969). Transient excitation of an elastic half space by a point load traveling on the surface, *J. Appl. Mech.* **36**; *Trans. ASME Ser. E*, **91**, 505–515.
- Hanson, M. E., A. R. Sanford, and R. J. Shaffer (1974). A source function for a dynamic brittle unilateral shear fracture, *Geophys. J.* **38**, 365–376.
- Haskell, N. A. (1969). Elastic displacements in the near-field of a propagating fault, *Bull. Seism. Soc. Am.* **59**, 865–908.
- Ida, Y. and K. Aki (1972). Seismic source-time function of propagating longitudinal-shear cracks, *J. Geophys. Res.* **77**, 2034–2044.
- Johnson, T., F. T. Wu, and C. H. Scholz (1973). Source parameters for stick-slip and for earthquakes, *Science* **179**, 278–280.
- Kostrov, B. V. (1964). Selfsimilar problems of propagation of shear cracks, *J. Appl. Math. Mech.* **28**, 1077–1087.
- Kostrov, B. V. (1966). Unsteady propagation of longitudinal shear cracks, *J. Appl. Math. Mech.* **30**, 1241–1248.
- Kostrov, B. V. and L. V. Nikitin (1970). Some general problems of mechanics of brittle fracture, *Arch. Mech. Stosowanej*, **22**, 749–776.
- Madariaga, R. (1975). Dependence of far-field radiation on source geometry, *E.O.S., Trans. Am. Geophys. Union* **56**, 400–401.
- McKenzie, D. and J. N. Brune (1972). Melting on fault planes during large earthquakes, *Geophys. J.* **29**, 65–78.
- Reid, H. F. (1910). Mechanics of the earthquake, in *The California Earthquake of April 18, 1906*, Vol. 2, Carnegie Inst. of Washington, D.C.
- Richards, P. G. (1973). The dynamic field of a growing plane elliptical shear crack, *Intern. J. Solids Structures* **9**, 843–861.
- Savage, J. C. (1965). The effect of rupture velocity upon seismic first motions, *Bull. Seism. Soc. Am.* **55**, 263–275.
- Savage, J. C. (1966). Radiation from a realistic model of faulting, *Bull. Seism. Soc. Am.* **56**, 577–592.

LAMONT DOHERTY GEOLOGICAL OBSERVATORY

AND

DEPARTMENT OF GEOLOGICAL SCIENCES

COLUMBIA UNIVERSITY

PALISADES, NEW YORK 10964

LAMONT-DOHERTY GEOLOGICAL OBSERVATORY CONTRIBUTION No. 2303.

Manuscript received July 21, 1975